Int. J. Appl. Math. Comput. Sci., 2004, Vol. 14, No. 4, 477–496

MODELING AND CONTROL OF A 4-WHEEL SKID-STEERING MOBILE ROBOT[†]

KRZYSZTOF KOZŁOWSKI*, DARIUSZ PAZDERSKI*

* Institute of Control and Systems Engineering
Poznań University of Technology
ul. Piotrowo 3A, 60–965 Poznań, Poland
e-mail: {Krzysztof.Kozlowski, Dariusz.Pazderski}@put.poznan.pl

A mathematical model of a 4-wheel skid-steering mobile robot is presented in a systematic way. The robot is considered as a subsystem consisting of kinematic, dynamic and drive levels. Next, a designing process of a kinematic controller based on the algorithm introduced by (Dixon *et al.*, 2001) is shown. An extension of the kinematic control law at the dynamic and motor levels using the Lyapunov analysis and the backstepping technique is developed. To validate the designed algorithm, extensive simulation results for trajectory tracking and set-point cases are discussed. Some deliberations concerning the tuning of the controller are presented, too.

Keywords: mobile robots, skid-steering vehicles, time-varying control laws, backstepping, Lyapunov analysis

1. Introduction

In recent years there has been observed a growing interest in the mobile robotics area. A lot of research concentrates on the description of kinematic models of mobile robots and designing feedback control laws for nonholonomic systems. Researchers typically consider wheeled platforms with nonholonomic constraints white assuming perfect rolling. An excellent overview concerning different types of these robots can be found in (Campion *et al.*, 1996).

Although significant research has been focused to path planning and motion control of nonholonomic vehicles, see, e.g., (Dixon *et al.*, 2001; 2003; Morin and Samson, 2003), research that examines and accommodates it for skid steering effects is sparse. Therefore, so far little has been written about the control of vehicles where a slippage phenomenon is necessary because of the drive mechanism. Such wheeled robots called skid-steering mobile robots (SSMRs) are considered as all-terrain vehicles because of the robust nature of the mechanical structure. They can work in hard environmental conditions and can be used, e.g., to explore space.

The steering of an SSMR is achieved by differentially driving wheel pairs on each side of the robot. Although the steering scheme yields some mechanical benefits, the control of an SSMR is a challenging task because the wheels must skid laterally to follow a curved path. If the projection of the instantaneous center of rotation (ICR) of the vehicle along the longitudinal axis becomes large, the vehicle can lose motion stability as a result of skidding. In contrast, this phenomenon is not important for traditional vehicles if only the no-slip assumption is satisfied.

Because of lateral skidding, velocity constraints occurring in SSMRs are quite different from the ones met in other mobile platforms where wheels are not supposed to skid. This implies that the control of this robot at the kinematic level only is not sufficient and, in general, demands the use of a properly designed control algorithm at the dynamic level, too.

Recently, Caracciolo *et al.* (1999) considered the motion stability problem of SSMRs and imposed an artificial operational constraint on the vehicle to limit the projection of the ICR onto the longitudinal axis to be confined to the wheelbase. They resolved the trajectory tracking case using a dynamic linearization of the SSMR model. However, due to the restriction imposed by the condition considered in (Brockett, 1983), the regulation problem was not solved. Robustness to unknown interaction ground forces of the designed controller was proved only for a straight line motion.

In this paper, the results obtained in (Caracciolo *et al.*, 1999) are extended to a new time differentiable and time-varying control scheme based on Dixon's kinematic controller. It allows us to solve both trajectory tracking and regulation problems and it is based on the strategy of forcing some transformed states to track an exogenous exponentially decaying signal produced by a tunable oscillator. This algorithm yields a global exponentially stable result for the transformed states and a global uniformly

[†] This work was supported by a statutory grant no. DS 93/121/04.

ultimately bounded (GUUB) result for the actual position and orientation tracking or regulation errors. It gives practical stabilization in the sense considered in (Morin and Samson, 2003), and combines good performance and robustness to disturbances. An excellent survey concerning various algorithms to control nonholonomic systems can be found in (Morin and Samson, 2002).

Motivated by practical issues such as a desire to accommodate for unknown ground interaction forces, a robust controller is developed that incorporates the uncertain dynamic model of an SSMR. Additionally, the control law which takes into account electrical properties of the drive system is obtained. The result of stability is proved using the Lyapunov technique. It is important to note that, in contrast to the previous work done by (Caracciolo *et al.*, 1999; Kozłowski and Pazderski, 2003; Pazderski *et al.*, 2004), the kinematic model of the SSMR is reformulated to make it more practical for control purposes.

The paper is organized as follows: In Section 2 an SSMR is decomposed into three subsystems which consist of kinematic, dynamic and drive levels. Next, in a systematic way, a model of the vehicle is presented. Section 3 focuses on the development of the controller using the backstepping method. A detailed calculation concerning the transformation of the SSMR kinematics into a new space is presented, too. Next, the control scheme on the dynamic level is obtained to ensure robustness to the uncertainty of dynamical parameters. Further, electrical properties of DC motors are included. Next, extensive simulation results considering trajectory tracking and setpoint cases are given. Finally, some remarks concerning the tuning of this controller are presented.

2. Model of an SSMR

In this section a mathematical description of an SSMR moving on a planar surface is formulated. To facilitate the analysis and subsequent control development, the vehicle is divided into three parts including kinematics, dynamics and drive subsystems. This approach is quite natural for most mobile robots powered by electrical motors (see Fig. 1). Additionally, it offers a possibility to develop a controller based on the backstepping technique.

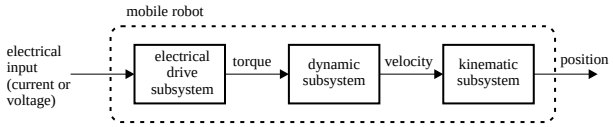

Fig. 1. Decomposition of an electrically driven mobile robot.

2.1. Kinematic Model

To consider the kinematic model of an SSMR, it is assumed that the robot is placed on a plane surface with the inertial orthonormal basis (X_g, Y_g, Z_g), see Fig. 2. A local coordinate frame denoted by (x_l, y_l, z_l) is assigned to the robot at its center of mass (COM). According to Fig. 2, the coordinates of COM in the inertial frame can be written as $\mathrm{COM} = (X, Y, Z)$. Since in this paper the plane motion is considered only, the Z-coordinate of COM is constant ($Z = \mathrm{const}$).

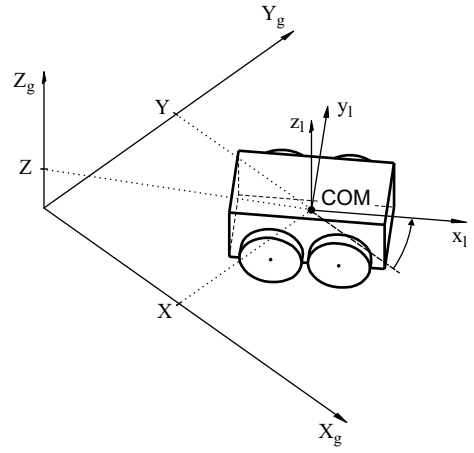

Fig. 2. SSMR in the inertial frame.

Suppose that the robot moves on a plane with linear velocity expressed in the local frame as $\boldsymbol{v} = [\ v_x \quad v_y \quad 0\ ]^T$ and rotates with an angular velocity vector $\boldsymbol{\omega} = [\ 0 \quad 0 \quad \omega\ ]^T$. If $\boldsymbol{q} = [\ X \quad Y \quad \theta\ ]^T$ is the state vector describing generalized coordinates of the robot (i.e., the COM position, X and Y, and the orientation θ of the local coordinate frame with respect to the inertial frame), then $\dot{\boldsymbol{q}} = [\ \dot{X} \quad \dot{Y} \quad \dot{\theta}\ ]^T$ denotes the vector of generalized velocities. From Fig. 3 it can be noted that the variables $\dot{X}$ and $\dot{Y}$ are related to the coordinates of the local velocity vector as follows (see Carac-

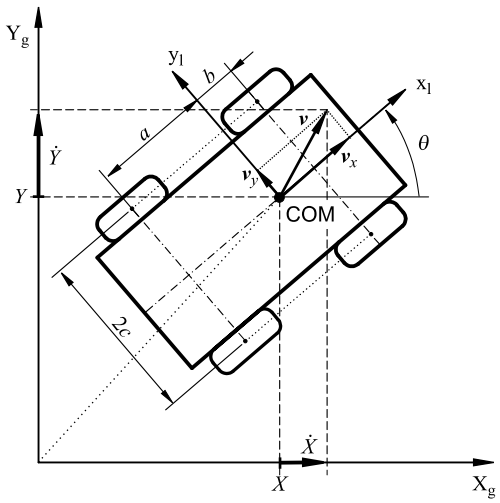

Fig. 3. Free body diagram.

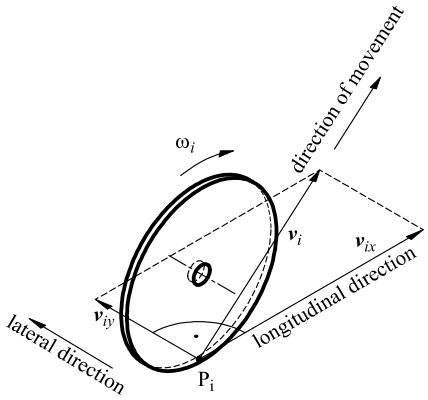

Fig. 4. Velocities of one wheel.

ciolo *et al.*, 1999):

$$\begin{bmatrix} \dot{X} \\ \dot{Y} \end{bmatrix} = \begin{bmatrix} \cos\theta & -\sin\theta \\ \sin\theta & \cos\theta \end{bmatrix} \begin{bmatrix} v_x \\ v_y \end{bmatrix}. \tag{1}$$

Furthermore, because of the planar motion, one can write $\dot{\theta} = \omega$.

It is obvious that Eqn. (1) does not impose any restrictions on the SSMR plane movement, since it describes free-body kinematics only. Therefore it is necessary to analyze the relationship between wheel velocities and local velocities.

Suppose that the i-th wheel rotates with an angular velocity $\omega_i\,(t)$, where $i = 1, 2, \ldots, 4,$ which can be seen as a control input. For simplicity, the thickness of the wheel is neglected and is assumed to be in contact with the plane at point P_i as illustrated in Fig. 4. In contrast to most wheeled vehicles, the lateral velocity of the SMRR, v_{iy}, is generally nonzero. This property comes from the mechanical structure of the SSMR that makes lateral skidding necessary if the vehicle changes its orientation. Therefore the wheels are tangent to the path only if $\omega = 0$, i.e., when the robot moves along a straight line.

In this description we consider only a simplified case of the SSMR movement for which the longitudinal slip between the wheels and the surface can be neglected. According to this assumption based on work done by (Pacejka, 2002), the following relation can be developed:

$$v_{ix} = r_i \omega_i, \tag{2}$$

where v_{ix} is the longitudinal component of the total velocity vector $\boldsymbol{v}_i$ of the i-th wheel expressed in the local frame and r_i denotes the so-called effective rolling radius of that wheel.

To develop a kinematic model, it is necessary to take into consideration all wheels together. In Fig. 5, the radius vectors $\boldsymbol{d}_i = [\ d_{ix} \quad d_{iy}\ ]^T$ and $\boldsymbol{d}_C = [\ d_{Cx} \quad d_{Cy}\ ]^T$

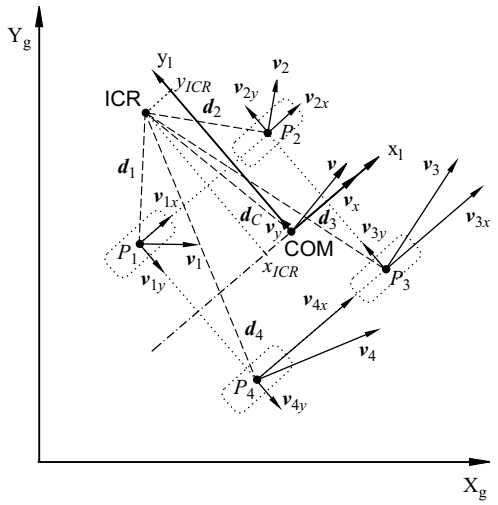

Fig. 5. Wheel velocities.

are defined with respect to the local frame from the instantaneous center of rotation (ICR). Consequently, based on the geometry of Fig. 5, the following expression can be deduced:

$$\frac{\|\boldsymbol{v}_i\|}{\|\boldsymbol{d}_i\|} = \frac{\|\boldsymbol{v}\|}{\|\boldsymbol{d}_C\|} = |\omega| \tag{3}$$

or, in a more detailed form,

$$\frac{v_{ix}}{-d_{iy}} = \frac{v_x}{-d_{Cy}} = \frac{v_{iy}}{d_{ix}} = \frac{v_y}{d_{Cx}} = \omega, \tag{4}$$

where the symbol $\|\cdot\|$ denotes the Euclidean norm.

Defining the coordinates of the ICR in the local frame as

$$\mathrm{ICR} = (x_{\mathrm{ICR}}, y_{\mathrm{ICR}}) = (-d_{xC}, -d_{yC}) \tag{5}$$

allows us to rewrite (4) as follows:

$$\frac{v_x}{y_{\mathrm{ICR}}} = -\frac{v_y}{x_{\mathrm{ICR}}} = \omega. \tag{6}$$

From Fig. 5 it is clear that the coordinates of vectors $\boldsymbol{d}_i$ satisfy the following relationships:

$$\begin{aligned} d_{1y} &= d_{2y} = d_{Cy} + c, \\ d_{3y} &= d_{4y} = d_{Cy} - c, \\ d_{1x} &= d_{4x} = d_{Cx} - a, \\ d_{2x} &= d_{3x} = d_{Cx} + b, \end{aligned} \tag{7}$$

where a, b and c are positive kinematic parameters of the robot depicted in Fig. 3. After combining Eqns. (4) and (7), the following relationships between wheel velocities can be obtained:

$$\begin{aligned} v_L &= v_{1x} = v_{2x}, \\ v_R &= v_{3x} = v_{4x}, \\ v_F &= v_{2y} = v_{3y}, \\ v_B &= v_{1y} = v_{4y}, \end{aligned} \tag{8}$$

where v_L and v_R denote the longitudinal coordinates of the left and right wheel velocities, v_F and v_B are the lateral coordinates of the velocities of the front and rear wheels, respectively.

Using (4)–(8) it is possible to obtain the following transformation describing the relationship between the wheel velocities and the velocity of the robot:

$$\begin{bmatrix} v_L \\ v_R \\ v_F \\ v_B \end{bmatrix} = \begin{bmatrix} 1 & -c \\ 1 & c \\ 0 & -x_{\mathrm{ICR}} + b \\ 0 & -x_{\mathrm{ICR}} - a \end{bmatrix} \begin{bmatrix} v_x \\ \omega \end{bmatrix}. \tag{9}$$

In accordance with (2) and (8), assuming that the effective radius is $r_i = r$ for each wheel, we can write

$$\boldsymbol{\omega}_w = \begin{bmatrix} \omega_L \\ \omega_R \end{bmatrix} = \frac{1}{r} \begin{bmatrix} v_L \\ v_R \end{bmatrix}, \tag{10}$$

where ω_L are ω_R are the angular velocities of the left and right wheels, respectively.

Combining (9) and (10), the following approximated relations between the angular wheel velocities and the velocities of the robot can be developed:

$$\boldsymbol{\eta} = \begin{bmatrix} v_x \\ \omega \end{bmatrix} = r \begin{bmatrix} \dfrac{\omega_L + \omega_R}{2} \\ \dfrac{-\omega_L + \omega_R}{2c} \end{bmatrix}, \tag{11}$$

where $\boldsymbol{\eta}$ is a new control input introduced at the kinematic level.

From the last equation it is clear that, theoretically, the pair of velocities ω_L and ω_R can be treated as a control kinematic input signal as well as velocities v_x and ω. However, the accuracy of the relation (11) mostly depends on the longitudinal slip and can be valid only if this phenomenon is not dominant. In addition, the parameters r and c may be identified experimentally to ensure a high validity of the determination of the angular robot velocity with respect to the angular velocities of the wheels.

To complete the kinematic model of the SSMR, the following velocity constraint introduced in (Caracciolo *et al.*, 1999) from (6) can be considered:

$$v_y + x_{\mathrm{ICR}} \dot{\theta} = 0. \tag{12}$$

The last equation is not integrable. In consequence, it describes a nonholonomic constraint which can be rewritten in the Pfaffian form:

$$\begin{bmatrix} -\sin\theta & \cos\theta & x_{\mathrm{ICR}} \end{bmatrix} \begin{bmatrix} \dot{X} & \dot{Y} & \dot{\theta} \end{bmatrix}^T = \boldsymbol{A}(\boldsymbol{q})\, \dot{\boldsymbol{q}} = \boldsymbol{0}, \tag{13}$$

where Eqn. (1) has been used. Since the generalized velocity $\dot{\boldsymbol{q}}$ is always in the null space of $\boldsymbol{A}$, we can write

$$\dot{\boldsymbol{q}} = \boldsymbol{S}(\boldsymbol{q})\, \boldsymbol{\eta}, \tag{14}$$

where

$$\boldsymbol{S}^T(\boldsymbol{q})\, \boldsymbol{A}^T(\boldsymbol{q}) = \boldsymbol{0} \tag{15}$$

and

$$\boldsymbol{S}(\boldsymbol{q}) = \begin{bmatrix} \cos\theta & x_{\mathrm{ICR}} \sin\theta \\ \sin\theta & -x_{\mathrm{ICR}} \cos\theta \\ 0 & 1 \end{bmatrix}. \tag{16}$$

It should be noted that since $\dim(\boldsymbol{\eta}) = 2 < \dim(\boldsymbol{q}) = 3$, Eqn. (14) describes the kinematics of the robot, which is underactuated. Additionally, this is a nonholonomic system because of the constraint described by (12). It is interesting to see that the analysed kinematic model of the SSMR is quite similar to the kinematics of the two-wheel mobile robot presented by (Kozłowski and Majchrzak, 2002).

From (6) and (9) it can be seen that control of the v_y and v_{yi} velocity coordinates is not possible without the knowledge of the x_l-axis projection of the ICR. Therefore, considering the linear velocity v_x and the angular velocity ω as control signals seems to have an advantage over the previous propositions presented by (Kozłowski and Pazderski, 2003; Caracciolo *et al.*, 1999), where instead of ω, the velocity v_y is used.

2.2. Dynamic Model

In this section the dynamic properties of the SSMR are described, since the dynamic effects play an important role for such vehicles (see Caracciolo *et al.*, 1999). It is caused by unknown lateral skidding ground interaction forces. First, the wheel forces depicted in Fig. 6 are examined.

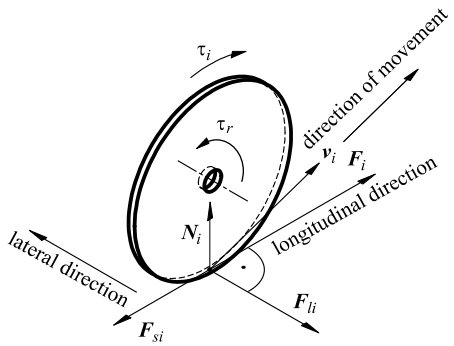

Fig. 6. Forces acting on one wheel.

The active force F_i and reactive force N_i are related to the wheel torque and gravity, respectively. It is clear

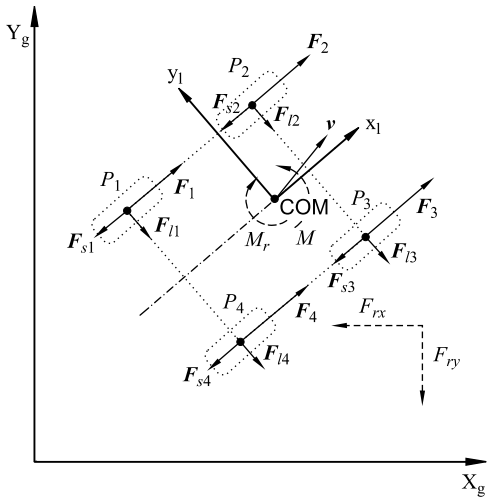

Fig. 7. Active and resistive forces of the vehicle.

that F_i is linearly dependent on the wheel control input τ_i, namely,

$$F_i = \frac{\tau_i}{r}. \tag{17}$$

According to (Pacejka, 2002) we assume that the vertical force N_i acts from the surface to the wheel. Considering the four wheels of the vehicle (Fig. 7) and neglecting additional dynamic properties, we obtain the following equations of equilibrium:

$$\begin{aligned} N_1 a &= N_2 b, \\ N_4 a &= N_3 b, \\ \sum_{i=1}^{4} N_i &= mg, \end{aligned} \tag{18}$$

where m denotes the vehicle mass and g is the gravity acceleration. Since there is symmetry along the longitudinal midline, we obtain

$$\begin{aligned} N_1 = N_4 &= \frac{b}{2\,(a+b)} mg, \\ N_2 = N_3 &= \frac{a}{2\,(a+b)} mg. \end{aligned} \tag{19}$$

Assume that the vector F_{si} results from the rolling resistant moment τ_{ri} and the vector F_{li} denotes the lateral reactive force. Based on (Caracciolo *et al.*, 1999) these reactive forces can be regarded as friction ones. However, it is important to note that friction modeling is quite complicated since it is highly nonlinear and depends on many variables. Therefore, in most cases only a simplified approximation describing the friction F_f as a superposition of Coulumb and viscous friction is considered. It can be written as

$$F_f(\sigma) = \mu_c N \operatorname{sgn}(\sigma) + \mu_v \sigma, \tag{20}$$

where σ denotes the linear velocity, N is the force perpendicular to the surface, while μ_c and μ_v denote the coefficients of Coulumb and viscous friction, respectively. Since for the SSMR the velocity σ is relatively low, especially during lateral slippage, the relation $\mu_c N \gg |\mu_v \sigma|$ is valid, which allows us to neglect the term $\mu_v \sigma$ to simplify the model. It is very important to note that the function (20) is not smooth when the velocity σ equals zero, because of the sign function $\operatorname{sgn}(\sigma)$. It is obvious that this function is not differentiable at $\sigma = 0$. Since a continuous and time differentiable model of the SSMR should be obtained, the following approximation of this function is proposed:

$$\widehat{\operatorname{sgn}}(\sigma) = \frac{2}{\pi} \arctan(k_s \sigma), \tag{21}$$

where $k_s \gg 1$ is a constant which determines the approximation accuracy according to the relation

$$\lim_{k_s \to \infty} \frac{2}{\pi} \arctan(k_s \sigma) = \operatorname{sgn}(x). \tag{22}$$

Based on the previous deliberations, the friction forces for one wheel can be written as

$$F_{li} = \mu_{lci} mg \widehat{\operatorname{sgn}}(v_{yi}), \tag{23}$$

$$F_{si} = \mu_{sci} mg \widehat{\operatorname{sgn}}(v_{xi}), \tag{24}$$

where μ_{lci} and μ_{sci} denote the coefficients of the lateral and longitudinal forces, respectively.

Using the Lagrange-Euler formula with Lagrange multipliers to include the nonholonomic constraint (12), the dynamic equation of the robot can be obtained. Next, it is assumed that the potential energy of the robot $PE(\boldsymbol{q}) = 0$ because of the planar motion. Therefore the Lagrangian L of the system equals the kinetic energy:

$$L(\boldsymbol{q}, \dot{\boldsymbol{q}}) = T(\boldsymbol{q}, \dot{\boldsymbol{q}}). \tag{25}$$

Considering the kinetic energy of the vehicle and neglecting the energy of rotating wheels, the following equation can be developed:

$$T = \frac{1}{2} m \boldsymbol{v}^T \boldsymbol{v} + \frac{1}{2} I \omega^2, \tag{26}$$

where m denotes the mass of the robot and I is the moment of inertia of the robot about the COM. For simplicity, it is assumed that the mass distribution is homogeneous. Since $\boldsymbol{v}^T \boldsymbol{v} = v_x^2 + v_y^2 = \dot{X}^2 + \dot{Y}^2$, Eqn. (26) can be rewritten in the following form:

$$T = \frac{1}{2} m \left(\dot{X}^2 + \dot{Y}^2 \right) + \frac{1}{2} I \dot{\theta}^2. \tag{27}$$

After calculating the partial derivative of kinetic energy and its time-derivative, the inertial forces can be obtained as

$$\frac{\mathrm{d}}{\mathrm{d}t}\left(\frac{\partial E_k}{\partial \dot{\boldsymbol{q}}}\right) = \begin{bmatrix} m\ddot{X} \\ m\ddot{Y} \\ I\ddot{\theta} \end{bmatrix} = \boldsymbol{M}\ddot{\boldsymbol{q}}, \tag{28}$$

where

$$\boldsymbol{M} = \begin{bmatrix} m & 0 & 0 \\ 0 & m & 0 \\ 0 & 0 & I \end{bmatrix}. \tag{29}$$

Consequently, the forces which cause the dissipation of energy are considered. According to Fig. 7, the following resultant forces expressed in the inertial frame can be calculated:

$$F_{rx}(\dot{\boldsymbol{q}}) = \cos\theta \sum_{i=1}^{4} F_{si}(v_{xi}) - \sin\theta \sum_{i=1}^{4} F_{li}(v_{yi}), \tag{30}$$

$$F_{ry}(\dot{\boldsymbol{q}}) = \sin\theta \sum_{i=1}^{4} F_{si}(v_{xi}) + \cos\theta \sum_{i=1}^{4} F_{li}(v_{yi}). \tag{31}$$

The resistant moment around the center of mass M_r can be obtained as

$$M_r(\dot{\boldsymbol{q}}) = -a \sum_{i=1,4} F_{li}(v_{yi}) + b \sum_{i=2,3} F_{li}(v_{yi}) + c\left[-\sum_{i=1,2} F_{si}(v_{xi}) + \sum_{i=3,4} F_{si}(v_{xi})\right]. \tag{32}$$

To define generalized resistive forces, the vector

$$\boldsymbol{R}(\dot{\boldsymbol{q}}) = \begin{bmatrix} F_{rx}(\dot{\boldsymbol{q}}) & F_{ry}(\dot{\boldsymbol{q}}) & M_r(\dot{\boldsymbol{q}}) \end{bmatrix}^T \tag{33}$$

is introduced. The active forces generated by the actuators which make the robot move can be expressed in the inertial frame as follows:

$$F_x = \cos\theta \sum_{i=1}^{4} F_i, \tag{34}$$

$$F_y = \sin\theta \sum_{i=1}^{4} F_i. \tag{35}$$

The active torque around the COM is calculated as

$$M = c(-F_1 - F_2 + F_3 + F_4). \tag{36}$$

In consequence, the vector $\boldsymbol{F}$ of active forces has the following form:

$$\boldsymbol{F} = \begin{bmatrix} F_x & F_y & M \end{bmatrix}^T. \tag{37}$$

Using (17), (34)–(36) and assuming that the radius of each wheel is the same, we get

$$\boldsymbol{F} = \frac{1}{r}\begin{bmatrix} \cos\theta \sum_{i=1}^{4} \tau_i \\ \sin\theta \sum_{i=1}^{4} \tau_i \\ c(-\tau_1 - \tau_2 + \tau_3 + \tau_4) \end{bmatrix}. \tag{38}$$

To simplify the notation, a new torque control input $\boldsymbol{\tau}$ is defined as

$$\boldsymbol{\tau} = \begin{bmatrix} \tau_L \\ \tau_R \end{bmatrix} = \begin{bmatrix} \tau_1 + \tau_2 \\ \tau_3 + \tau_4 \end{bmatrix}, \tag{39}$$

where τ_L and τ_R denote the torques produced by the wheels on the left and right sides of the vehicle, respectively. Combining (38) and (39), we get

$$\boldsymbol{F} = \boldsymbol{B}(\boldsymbol{q})\boldsymbol{\tau}, \tag{40}$$

where $\boldsymbol{B}$ is the input transformation matrix defined as

$$\boldsymbol{B}(\boldsymbol{q}) = \frac{1}{r}\begin{bmatrix} \cos\theta & \cos\theta \\ \sin\theta & \sin\theta \\ -c & c \end{bmatrix}. \tag{41}$$

Next, using (28), (33) and (40), the following dynamic model is obtained:

$$\boldsymbol{M}(\boldsymbol{q})\ddot{\boldsymbol{q}} + \boldsymbol{R}(\dot{\boldsymbol{q}}) = \boldsymbol{B}(\boldsymbol{q})\boldsymbol{\tau}. \tag{42}$$

It should be noted that (42) describes the dynamics of a free body only and does not include the nonholonomic constraint (13). Therefore a constraint has to be imposed on (42). To this end, a vector of Lagrange multipliers, $\boldsymbol{\lambda}$, is introduced as follows (see Caracciolo *et al.*, 1999; Gutowski, 1971):

$$\boldsymbol{M}(\boldsymbol{q})\ddot{\boldsymbol{q}} + \boldsymbol{R}(\dot{\boldsymbol{q}}) = \boldsymbol{B}(\boldsymbol{q})\boldsymbol{\tau} + \boldsymbol{A}^T(\boldsymbol{q})\boldsymbol{\lambda}. \tag{43}$$

For control purposes it would be more suitable to express (43) in terms of the internal velocity vector $\boldsymbol{\eta}$. Therefore, (43) is multiplied from the left by $\boldsymbol{S}^T(\boldsymbol{q})$, which results in

$$\boldsymbol{S}^T(\boldsymbol{q})\boldsymbol{M}(\boldsymbol{q})\ddot{\boldsymbol{q}} + \boldsymbol{S}^T(\boldsymbol{q})\mathbf{R}(\dot{\mathbf{q}}) = \boldsymbol{S}(\boldsymbol{q})^T\boldsymbol{B}(\boldsymbol{q})\boldsymbol{\tau} + \boldsymbol{S}^T(\boldsymbol{q})\boldsymbol{A}^T(\boldsymbol{q})\boldsymbol{\lambda}. \tag{44}$$

After taking the time derivative of (14), we obtain

$$\ddot{\boldsymbol{q}} = \dot{\boldsymbol{S}}(\boldsymbol{q})\boldsymbol{\eta} + \boldsymbol{S}(\boldsymbol{q})\dot{\boldsymbol{\eta}}. \tag{45}$$

Next, using (45) and (14) in (43), the dynamic equations become

$$\bar{\boldsymbol{M}}\dot{\boldsymbol{\eta}} + \bar{\boldsymbol{C}}\boldsymbol{\eta} + \bar{\boldsymbol{R}} = \bar{\boldsymbol{B}}\boldsymbol{\tau}, \tag{46}$$

where

$$\bar{\boldsymbol{C}} = \boldsymbol{S}^T \boldsymbol{M} \dot{\boldsymbol{S}} = m x_{\mathrm{ICR}} \begin{bmatrix} 0 & \dot{\theta} \\ -\dot{\theta} & \dot{x}_{\mathrm{ICR}} \end{bmatrix} \quad (47)$$

$$\bar{\boldsymbol{M}} = \boldsymbol{S}^T \boldsymbol{M} \boldsymbol{S} = \begin{bmatrix} m & 0 \\ 0 & m x_{\mathrm{ICR}}^2 + I \end{bmatrix}, \quad (48)$$

$$\bar{\boldsymbol{R}} = \boldsymbol{S}^T \boldsymbol{R} = \begin{bmatrix} F_{rx}(\dot{\boldsymbol{q}}) \\ x_{\mathrm{ICR}} F_{ry}(\dot{\boldsymbol{q}}) + M_r \end{bmatrix}, \quad (49)$$

$$\bar{\boldsymbol{B}} = \boldsymbol{S}^T \boldsymbol{B} = \frac{1}{r} \begin{bmatrix} 1 & 1 \\ -c & c \end{bmatrix}. \quad (50)$$

2.3. Drive Model of the SSMR

In this section a model of the SSMR drive is developed. It is assumed that the robot is driven by four DC brushed motors with mechanical gears. In Fig. 8 a simplified scheme of the drive on the right side of the robot is depicted. Considering only one drive and assuming for simplicity that the torque τ_{mi} produced by the i-th motor is linearly dependent on the rotor current i_{ai}, we can write

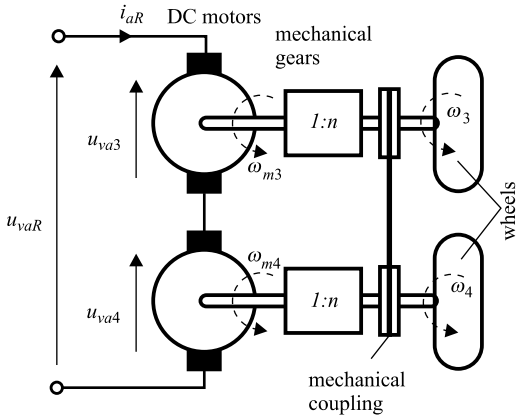

Fig. 8. Drive system on the right side of the vehicle.

$$\tau_{mi} = k_i i_{ai}, \quad (51)$$

where k_i denotes a motor torque constant. The voltage equation of the armature can be approximated by the following linear relationship:

$$u_{iva} = L_a \frac{\mathrm{d}}{\mathrm{d}t} i_{ai} + R_a i_{ai} + k_e \omega_{mi}, \quad (52)$$

where L_a and R_a denote the series inductance and resistance of the rotors, respectively, k_e is the electromotive force coefficient, while ω_{mi} denotes the angular velocity of the rotor. Since the i-th actuator is equipped with gears characterized by a ratio $n > 1$, we get

$$\tau_i = n k_i i_{ai}, \quad (53)$$

$$\omega_{mi} = n \omega_i, \quad (54)$$

where some additional dynamic effects concerning inertia and backlash of gears have been neglected. According to Fig. 8, a new input control signal $\boldsymbol{u}_{va}$ on the voltage level is defined as

$$\boldsymbol{u}_{va} = \begin{bmatrix} u_{vaL} & u_{vaR} \end{bmatrix}^T, \quad (55)$$

where u_{vaL} and u_{vaR} denote the motor voltage signals on the left and right sides of the vehicle, respectively. Since each pair of motors is electrically and mechanically coupled, we have

$$\begin{bmatrix} u_{vaL} \\ u_{vaR} \end{bmatrix} = \begin{bmatrix} u_{va1} + u_{va2} \\ u_{va3} + u_{va4} \end{bmatrix} \quad (56)$$

and

$$\begin{bmatrix} \omega_L \\ \omega_R \end{bmatrix} = \frac{1}{n} \begin{bmatrix} \omega_{m1} \\ \omega_{m3} \end{bmatrix} = \frac{1}{n} \begin{bmatrix} \omega_{m2} \\ \omega_{m4} \end{bmatrix}. \quad (57)$$

Assuming that all motors and gears have the same parameters and using (51)–(57), the following voltage-current equations are developed:

$$\boldsymbol{\tau} = 2 k_i n \boldsymbol{i}_a, \quad (58)$$

$$\boldsymbol{u}_{va} = 2 L_a \frac{\mathrm{d}}{\mathrm{d}t} \boldsymbol{i}_a + 2 R_a \boldsymbol{i}_a + 2 k_e n \boldsymbol{\omega}_w. \quad (59)$$

3. Control Law

In this section an algorithm which solves the regulation and trajectory tracking problem is considered. First, according to (Caracciolo *et al.*, 1999), an operational nonholonomic constraint (see Gutowski, 1971) is introduced to limit the magnitude of lateral slippage in open loop control. Second, the idea of a kinematic oscillator proposed by (Dixon *et al.*, 2001) is used. Finally, the proposed control scheme consists of kinematic, dynamic and motor levels, which ensures a better performance of the overall algorithm.

3.1. Operational Constraint

It is easy to observe that the ICR position influences the motion of the SSMR. In contrast to most mobile robots where the wheels are not supposed to skid, the ICR of the SSMR is not fixed. Therefore, theoretically, it can move

during the robot motion. However, it can be seen from Fig. 5 and Eqn. (9) that if the x_{ICR} coordinate goes out, of the robot wheelbase, then the robot skids into a lateral direction and loses its stability.

To solve this problem, Caracciolo *et al.* (1999) proposed to include an operational nonholonomic constraint (mathematical constraint) which is based on (12). This constraint can be written as

$$v_y + x_0\dot{\theta} = 0, \tag{60}$$

where x_0 denotes a fixed coordinate of the ICR which should be selected as

$$x_0 \in (-a, b)\,. \tag{61}$$

It can be interpreted as a programmable limitation of the SSMR lateral skidding that is done by imposing the constraint on the kinematic and dynamic model of the vehicle. To this end, x_{ICR} in (16), (47)–(50) is replaced by x_0 and it is assumed that $\dot{x}_{\mathrm{ICR}} = 0$. In consequence, the matrix $\boldsymbol{S}(\boldsymbol{q})$ becomes

$$\boldsymbol{S}(\boldsymbol{q}) = \begin{bmatrix} \cos\theta & x_0\sin\theta \\ \sin\theta & -x_0\cos\theta \\ 0 & 1 \end{bmatrix}. \tag{62}$$

The value of x_0 is arbitrarily chosen and belongs to the set defined by (61). It is not related to any structural properties of the SSMR. It is just a coefficient which allows us to approximate the relation between the angular and linear lateral velocities of the robot. It is interesting to see that selecting $x_0 = 0$ makes the SSMR kinematics model similar to the kinematics of a typical two-wheel robot.

3.2. Control Objective

The vector of the position and orientation error $\tilde{\boldsymbol{q}}$ is defined as follows:

$$\tilde{\boldsymbol{q}} = \boldsymbol{q} - \boldsymbol{q}_r = \begin{bmatrix} \tilde{X} & \tilde{Y} & \tilde{\theta} \end{bmatrix}^T, \tag{63}$$

where $\boldsymbol{q}_r = [\ X_r \quad Y_r \quad \theta_r\ ]^T$ denotes the desired position, X_r and Y_r, of the COM and the desired orientation θ_r. It should be noted that in the case of the regulation problem we have $\boldsymbol{q}_r = \mathrm{const}$. However, for the trajectory tracking problem, $\boldsymbol{q}_r(t)$ is a vector function which depends explicitly on time. In the second case, $\boldsymbol{q}_r(t)$ denotes a reference trajectory, generated by a reference kinematic model with an operational constraint (60) as follows:

$$\dot{\boldsymbol{q}}_r(t) = \boldsymbol{S}\big[\boldsymbol{q}_r(t)\big]\boldsymbol{\eta}_r(t)\,, \tag{64}$$

where $\boldsymbol{S}(\cdot)$ is defined by (16), and $\boldsymbol{\eta}_r(t) = [\ v_{rx}(t) \quad \omega_r(t)\ ]^T$ denotes the reference velocity vector. All reference signals and their derivatives are assumed to be bounded for all times:

$$\boldsymbol{\eta}_r(t)\,, \dot{\boldsymbol{\eta}}_r(t)\,, \boldsymbol{q}_r(t)\,, \dot{\boldsymbol{q}}_r(t) \in \mathscr{L}_\infty. \tag{65}$$

The control objective is formulated as a practical stabilization of the position and the orientation of the robot considered in (Morin and Samson, 2003) in the sense that

$$\lim_{t\to\infty} \|\tilde{\boldsymbol{q}}(t)\| \le \epsilon, \tag{66}$$

where ϵ denotes an arbitrary small positive constant.

3.3. Kinematic Transformation

In this section we introduce a kinematic transformation which will be used later on in designing a control law. Calculating a time derivative of (63), we obtain the following kinematic error equation:

$$\dot{\tilde{\boldsymbol{q}}} = \dot{\boldsymbol{q}} - \dot{\boldsymbol{q}}_r. \tag{67}$$

Using (14) and (64), we get

$$\dot{\tilde{\boldsymbol{q}}} = \boldsymbol{S}(\boldsymbol{q})\,\boldsymbol{\eta} - \boldsymbol{S}(\boldsymbol{q}_r)\,\boldsymbol{\eta}_r. \tag{68}$$

Taking into account (62), we reformulate (68) as follows:

$$\dot{\tilde{\boldsymbol{q}}} = \boldsymbol{g}_0 + \boldsymbol{g}_1(\boldsymbol{q})\,v_x + \boldsymbol{g}_2(\boldsymbol{q})\,\omega, \tag{69}$$

where v_x and ω are control inputs, $\boldsymbol{g}_0$ is a drift of the system, $\boldsymbol{g}_1(\boldsymbol{q})$ and $\boldsymbol{g}_2(\boldsymbol{q})$ are vector field generators:

$$\boldsymbol{g}_0(\boldsymbol{q}_r) = -\boldsymbol{S}(\boldsymbol{q}_r)\,\boldsymbol{\eta}_r, \tag{70}$$

$$\boldsymbol{g}_1(\boldsymbol{q}) = \begin{bmatrix} \cos\theta \\ \sin\theta \\ 0 \end{bmatrix}, \tag{71}$$

$$\boldsymbol{g}_2(\boldsymbol{q}) = \begin{bmatrix} x_0\sin\theta \\ -x_0\cos\theta \\ 1 \end{bmatrix}. \tag{72}$$

From (70) it is clear that the drift is caused by the reference kinematics signals and for $\boldsymbol{\eta}_r = \boldsymbol{0}$ (i.e., when the regulation problem is considered) the system has no drift. Furthermore, the system expressed by (69) is underactuated since $\dim(\boldsymbol{\eta}) = 2 < \dim(\tilde{\boldsymbol{q}}) = 3$.

In order to build a kinematic controller based on (Dixon *et al.*, 2001), (68) is transformed into a form which is similar to the nonholonomic integrator considered in (Brockett, 1983):

$$\dot{w} = \boldsymbol{u}^T\boldsymbol{J}^T\boldsymbol{z} + f, \tag{73}$$

$$\dot{\boldsymbol{z}} = \boldsymbol{u}, \tag{74}$$

where w and $\boldsymbol{z} = [\ z_1 \quad z_2\ ]^T$ denote auxiliary variables, $\boldsymbol{u}$ is an input signal and f denotes the drift, while $\boldsymbol{J}$ is the following skew-symmetric matrix:

$$\boldsymbol{J} = \begin{bmatrix} 0 & -1 \\ 1 & 0 \end{bmatrix}. \tag{75}$$

It should be noted that the systems described by (68), (73) and (74) are first-order systems (see Murray and Sastry, 1993). It is possible to find the following global diffeomorfism that preserves the origin:

$$\boldsymbol{Z} = \begin{bmatrix} w & z_1 & z_2 \end{bmatrix}^T = \boldsymbol{P}\left(\theta, \tilde{\theta}\right)\tilde{\boldsymbol{q}}. \tag{76}$$

The variables w and $\boldsymbol{z}$ can be interpreted as a new auxiliary state vector of the system (68) described in a three-dimensional space.

To develop the transformation matrix $\boldsymbol{P}(\theta, \tilde{\theta})$, the regulation problem is considered first, i.e., $\boldsymbol{q}_r\,(t) = \mathbf{const}$. Then (73) can be rewritten as

$$\dot{w} = z_2 u_1 - z_1 u_2. \tag{77}$$

Based on (De Luca and Oriolo, 1995), the following change of coordinates is proposed:

$$z_1 = \tilde{\theta}, \tag{78}$$

$$z_2 = \tilde{X}\cos\theta + \tilde{Y}\sin\theta. \tag{79}$$

Observe that both of the new variables have a nice geometric interpretation: z_1 is the orientation error and $|z_2|$ denotes the length of projection of the vector $[\ \tilde{X} \quad \tilde{Y}\ ]^T$ onto the direction determined by the actual orientation θ (see Fig. 9).

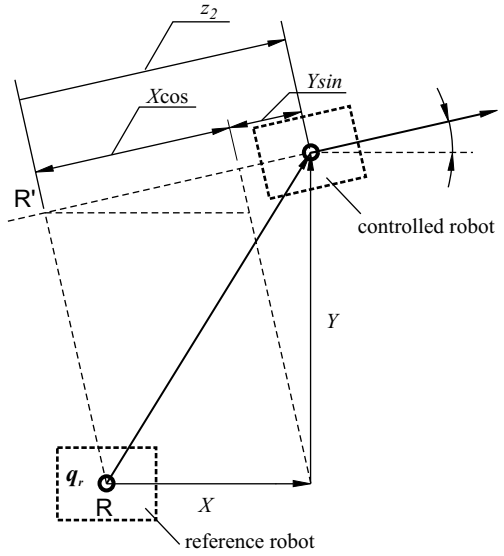

Fig. 9. Geometrical interpretation of the z_2 variable.

Taking the time derivative of (78) and (79), we can write

$$\dot{z}_1 = \dot{\tilde{\theta}}, \tag{80}$$

$$\dot{z}_2 = \frac{\mathrm{d}}{\mathrm{d}t}\left(\tilde{X}\cos\theta + \tilde{Y}\sin\theta\right). \tag{81}$$

Next, using (74), (80) and (81) in (77), it follows that

$$\dot{w} = \dot{\tilde{\theta}}\left(\tilde{X}\cos\theta + \tilde{Y}\sin\theta\right) - \tilde{\theta}\frac{\mathrm{d}}{\mathrm{d}t}\left(\tilde{X}\cos\theta + \tilde{Y}\sin\theta\right) \tag{82}$$

or

$$\dot{w} = \frac{\mathrm{d}}{\mathrm{d}t}\left[-\tilde{\theta}\left(\tilde{X}\cos\theta + \tilde{Y}\sin\theta\right)\right] + 2\dot{\tilde{\theta}}\left(\tilde{X}\cos\theta + \tilde{Y}\sin\theta\right). \tag{83}$$

Therefore the variable w can be expressed as

$$w = -\tilde{\theta}\left(\tilde{X}\cos\theta + \tilde{Y}\sin\theta\right) + 2\int\dot{\tilde{\theta}}\,(t)\left[\tilde{X}\,(t)\cos\theta\,(t) + \tilde{Y}\,(t)\sin\theta\,(t)\right]\mathrm{d}t. \tag{84}$$

To calculate the integral in (84), it is convenient to consider the expression

$$\frac{\mathrm{d}}{\mathrm{d}t}\left(\tilde{X}\sin\theta - \tilde{Y}\cos\theta\right) = \dot{\theta}\left(\tilde{X}\cos\theta + \tilde{Y}\sin\theta\right) + \dot{\tilde{X}}\sin\theta - \dot{\tilde{Y}}\cos\theta. \tag{85}$$

Using the error kinematics given by (68) and assuming that $v_{rx} = 0$ and $\omega_r = 0$, we see (note that it is just Eqn. (13) in the case of regulation) that

$$\dot{\tilde{X}}\sin\theta - \dot{\tilde{Y}}\cos\theta = x_0\dot{\tilde{\theta}}. \tag{86}$$

Then (85) can be rewritten as

$$\frac{\mathrm{d}}{\mathrm{d}t}\left(\tilde{X}\sin\theta - \tilde{Y}\cos\theta - x_0\tilde{\theta}\right) = \dot{\theta}\left(\tilde{X}\cos\theta + \tilde{Y}\sin\theta\right) = \dot{\tilde{\theta}}\left(\tilde{X}\cos\theta + \tilde{Y}\sin\theta\right). \tag{87}$$

Finally, according to (84), the variable w has the following form:

$$w = -\tilde{\theta}\left(\tilde{X}\cos\theta + \tilde{Y}\sin\theta\right) + 2\left(\tilde{X}\sin\theta - \tilde{Y}\cos\theta - x_0\tilde{\theta}\right). \tag{88}$$

Next, we calculate the term f which appears in (73). To this end, the trajectory tracking case is considered. Taking again the time derivative of (88), we conclude that

$$\begin{aligned}\dot{w} &= -\dot{\tilde{\theta}}\left(\tilde{X}\cos\theta+\tilde{Y}\sin\theta\right)\\ &\quad+\tilde{\theta}\left[\dot{\theta}\left(\tilde{X}\sin\theta-\tilde{Y}\cos\theta\right)-\dot{\tilde{X}}\cos\theta-\dot{\tilde{Y}}\sin\theta\right]\\ &\quad+2\dot{\theta}\left(\tilde{X}\cos\theta+\tilde{Y}\sin\theta\right)\\ &\quad+2\left(\dot{\tilde{X}}\sin\theta-\dot{\tilde{Y}}\cos\theta\right)-2x_0\dot{\tilde{\theta}}. \qquad (89)\end{aligned}$$

Using (68), (78) and (79) in (89), we have

$$\begin{aligned}\dot{w} &= -\dot{\tilde{\theta}}z_2-z_1\dot{z}_2+2\dot{\theta}z_2\\ &\quad+2\left(x_0\dot{\theta}-v_{rx}\sin z_1-x_0\omega_r\cos z_1\right)\\ &\quad-2x_0\dot{\theta}+2x_0\omega_r\\ &=\dot{\theta}z_2+\dot{\theta}_r z_2-2\dot{\theta}_r z_2+2\dot{\theta}_r z_2-z_1\dot{z}_2\\ &\quad+2\left(x_0\omega_r-v_{rx}\sin z_1-x_0\omega_r\cos z_1\right)\\ &=\dot{\tilde{\theta}}z_2-z_1\dot{z}_2+2\dot{\theta}_r z_2\\ &\quad+2\left(x_0\omega_r-v_{rx}\sin z_1-x_0\omega_r\cos z_1\right)\\ &=\dot{z}_1 z_2-z_1\dot{z}_2+2z_2\omega_r\\ &\quad+2\left(x_0\omega_r-v_{rx}\sin z_1-x_0\omega_r\cos z_1\right). \qquad (90)\end{aligned}$$

Next, substituting (74) into Eqn. (90) results in

$$\begin{aligned}\dot{w} &= u_1 z_2-z_1u_2\\ &\quad+2\left(z_2\omega_r+x_0\omega_r-v_{rx}\sin z_1-x_0\omega_r\cos z_1\right)\\ &=u_1z_2-z_1u_2\\ &\quad+2\left[-v_{rx}\sin z_1+\omega_r\left(x_0+z_2-x_0\cos z_1\right)\right], \qquad (91)\end{aligned}$$

and therefore

$$f=2\left[-v_{rx}\sin z_1+\omega_r\left(x_0+z_2-x_0\cos z_1\right)\right]. \qquad (92)$$

Summarizing, the matrix $\boldsymbol{P}$ in (76), which transforms (68) into (73)–(74), can be written as

$$\boldsymbol{P}\left(\theta,\tilde{\theta}\right)=\begin{bmatrix}-\tilde{\theta}\cos\theta+2\sin\theta & -\tilde{\theta}\sin\theta-2\cos\theta & -2x_0\\ 0 & 0 & 1\\ \cos\theta & \sin\theta & 0\end{bmatrix}. \qquad (93)$$

One can easily check that this matrix is nonsingular.

The velocity transformation can be obtained from (74) and (80)–(81) as follows:

$$\boldsymbol{u}=\boldsymbol{T}^{-1}\boldsymbol{\eta}-\begin{bmatrix}\omega_r\\ v_{rx}\cos z_1-x_0\omega_r\sin z_1\end{bmatrix}, \qquad (94)$$

where

$$\boldsymbol{T}^{-1}=\begin{bmatrix}0 & 1\\ 1 & -l\end{bmatrix} \quad \text{or} \quad \boldsymbol{T}=\begin{bmatrix}l & 1\\ 1 & 0\end{bmatrix} \qquad (95)$$

and $l=\tilde{X}\sin\theta-\tilde{Y}\cos\theta$ is an auxiliary variable that has the meaning of a distance. Based on (94), the velocity vector $\boldsymbol{\eta}$ can be expressed as

$$\boldsymbol{\eta}=\boldsymbol{T}\boldsymbol{u}+\boldsymbol{\Pi}, \qquad (96)$$

where

$$\boldsymbol{\Pi}=\begin{bmatrix}v_{rx}\cos z_1+\omega_r\left(-x_0\sin z_1+l\right)\\ \omega_r\end{bmatrix} \qquad (97)$$

is an auxiliary velocity vector which is nonzero only for the trajectory tracking problem when the reference velocity vector $\boldsymbol{\eta}_r\neq\boldsymbol{0}$.

3.4. Kinematic Control Law

In this section a kinematic control structure based on (Dixon *et al.*, 2001) which solves a unified tracking and regulation problem is proposed.

The control law has the following form:

$$\boldsymbol{u}=\boldsymbol{u}_a-k_2\boldsymbol{z}, \qquad (98)$$

where $\boldsymbol{u}_a$, which introduces a time-varying feedback to overcome Brockett's obstruction (see Brockett, 1983), is defined as

$$\boldsymbol{u}_a=\frac{k_1w+f}{\delta_d^2}\boldsymbol{J}\boldsymbol{z}_d+\Omega_1\boldsymbol{z}_d. \qquad (99)$$

From (99) it is clear that the signal $\boldsymbol{u}_a$ is modulated by an auxiliary signal $\boldsymbol{z}_d$ generated by the tunable oscillator described by the following linear non-stationary differential equation:

$$\dot{\boldsymbol{z}}_d=\frac{\dot{\delta}_d}{\delta_d}\boldsymbol{z}_d+\left(\frac{k_1w+f}{\delta_d^2}+w\Omega_1\right)\boldsymbol{J}\boldsymbol{z}_d, \qquad (100)$$

where $\boldsymbol{z}_d=\begin{bmatrix} z_{d1} & z_{d2}\end{bmatrix}^T$, Ω_1 and δ_d are auxiliary terms defined as

$$\Omega_1=k_2+\frac{\dot{\delta}_d}{\delta_d}+w\frac{k_1w+f}{\delta_d^2}, \qquad (101)$$

$$\delta_d=\alpha_0\exp\left(-\alpha_1 t\right)+\epsilon_1, \qquad (102)$$

while k_1, k_2, α_0, α_1 and ϵ_1 are positive constant design parameters.

It is easy to show that the envelope of $\|\boldsymbol{z}_d(t)\|$ is determined by the scalar function δ_d. In order to prove it,

we calculate the time derivative of the quadratic norm of the vector $\boldsymbol{z}_d(t)$ and next use (100) to obtain

$$\frac{\mathrm{d}}{\mathrm{d}t}\left(\boldsymbol{z}_d^T\boldsymbol{z}_d\right) = 2\frac{\dot{\delta}_d}{\delta_d}\boldsymbol{z}_d^T\boldsymbol{z}_d. \tag{103}$$

The solution of (103) can be written as

$$\boldsymbol{z}_d(t)^T\boldsymbol{z}_d(t) = \boldsymbol{z}_d(0)^T\boldsymbol{z}_d(0) = \delta_d^2(t). \tag{104}$$

Assuming that $\boldsymbol{z}_d(0)^T\boldsymbol{z}_d(0) = \delta_d^2(0)$, the envelope of $\|\boldsymbol{z}_d(t)\|$ is described by

$$\forall t \geq 0 \ \ \|\boldsymbol{z}_d(t)\| = \delta_d(t). \tag{105}$$

Theorem 1. *Provided that the reference trajectory is selected to be bounded for all times $t > 0$ (see (65)) and assuming that the kinematic model satisfies the constraint given by (60), the kinematic control law given by (98)–(102) ensures that the position and orientation errors defined by (63) are globally uniformly ultimately bounded as follows:*

$$\|\tilde{\boldsymbol{q}}\| \leq \kappa_0 \exp(-\kappa_1 t) + \kappa_2\epsilon_1, \tag{106}$$

where ϵ_1 can be made arbitrarily small, and κ_0, κ_1 and κ_2 are some positive constants.

A detailed proof of exponential stability to a small neighborhood of the equilibrium point is given by (Dixon *et al.*, 2001) and is based on the Lyapunov stability theory. The proposed Lyapunov function candidate has the following form:

$$V_1(w, \tilde{\boldsymbol{z}}) = \frac{1}{2}w^2 + \frac{1}{2}\tilde{\boldsymbol{z}}^T\tilde{\boldsymbol{z}}, \tag{107}$$

where $\tilde{\boldsymbol{z}} = \boldsymbol{z}_d - \boldsymbol{z}$ is an auxiliary error signal.

The derivation of differential equation errors governing w and $\tilde{\boldsymbol{z}}$ for the closed-loop kinematic controller can be found in (Dixon *et al.*, 2001). Using it, we get

$$\dot{V}_1(w, \tilde{\boldsymbol{z}}) = -k_1w^2 - k_2\tilde{\boldsymbol{z}}^T\tilde{\boldsymbol{z}}. \tag{108}$$

Since all signals of the controlled system are bounded (Dixon *et al.*, 2001), it can be proved that the errors w and $\tilde{\boldsymbol{z}}$ are exponentially driven to zero. This means that the signal $\boldsymbol{z}$ tends to an oscillator signal $\boldsymbol{z}_d$ whose norm approaches the constant ϵ_1 (c.f. (102)).

Remark 1. The parameters α_0, α_1 and ϵ_1 play a very important role in the controller tuning process. Since (105) is satisfied and $\lim_{t\to\infty}\boldsymbol{z}(t) = \boldsymbol{z}_d(t)$, the scalar function $\delta_d(t)$ allows us to influence all transient states. In this way, $\delta_d(t)$ can be seen as a function used for motion planning. It is essential if the initial error is quite high and the vehicle has velocity limitations. A similar meaning is attributed to the relation between the oscillator signals z_{d1} and z_{d2}, which determine the phase condition. According to (105), it is convenient to introduce the following parametrization:

$$\boldsymbol{z}_d(0) = \delta_d(0)\begin{bmatrix}\cos\varphi\\ \sin\varphi\end{bmatrix}, \tag{109}$$

where $\varphi \in (-\pi, \pi]$.

3.5. Dynamic Control Law

In this section an extension of the presented kinematic control law is developed by considering a dynamic model of the SSMR. It is motivated by the desire to improve the robustness of the control design. In this case, using a method which relies on linearizing the dynamic equations is not possible because of unknown lateral skidding forces. Instead, a controller which is robust to the dynamic unmodelled disturbances is designed. Since all kinematic signals are time differentiable, it is possible to incorporate dynamical properties using a Lyapunov analysis and the backstepping technique.

First, to facilitate the subsequent development and analysis, the dynamic equation (46) is transformed by substituting every occurrence of $\boldsymbol{\eta}$, $\dot{\boldsymbol{\eta}}$ by $\boldsymbol{u}$, $\dot{\boldsymbol{u}}$, respectively. Next, multiplying (46) from the right by $\boldsymbol{T}^T$, we get

$$\bar{\bar{\boldsymbol{M}}}\dot{\boldsymbol{u}} + \bar{\bar{\boldsymbol{C}}}\boldsymbol{u} + \bar{\bar{\boldsymbol{R}}} = \bar{\bar{\boldsymbol{B}}}\boldsymbol{\tau}, \tag{110}$$

where

$$\begin{aligned}&\bar{\bar{\boldsymbol{M}}} = \boldsymbol{T}^T\bar{\boldsymbol{M}}\boldsymbol{T}, && \bar{\bar{\boldsymbol{C}}} = \boldsymbol{T}^T\left(\bar{\boldsymbol{C}}\boldsymbol{T} + \bar{\boldsymbol{M}}\dot{\boldsymbol{T}}\right),\\ &\bar{\bar{\boldsymbol{R}}} = \boldsymbol{T}^T\left(\bar{\boldsymbol{C}}\boldsymbol{\Pi} + \bar{\boldsymbol{M}}\dot{\boldsymbol{\Pi}} + \bar{\boldsymbol{R}}\right), && \bar{\bar{\boldsymbol{B}}} = \boldsymbol{T}^T\bar{\boldsymbol{B}}.\end{aligned} \tag{111}$$

Remark 2. Based on the Rayleigh-Ritz theorem (Dixon *et al.*, 2003) and using the fact that $\bar{\bar{\boldsymbol{M}}}$ is a symmetric and positive definite matrix, the following inequality can be written:

$$\frac{1}{m_1(w, \boldsymbol{z})}\boldsymbol{\xi}^T\boldsymbol{\xi} \leq \boldsymbol{\xi}^T\bar{\bar{\boldsymbol{M}}}^{-1}\boldsymbol{\xi} \leq \frac{1}{m_2(w, \boldsymbol{z})}\boldsymbol{\xi}^T\boldsymbol{\xi}, \tag{112}$$

where $\boldsymbol{\xi} \in \mathbb{R}^2$, $m_1(w, \boldsymbol{z})$ and $m_2(w, \boldsymbol{z})$ are positive scalar functions dependent on the actual tracking errors which denote the actual minimum and maximum eigenvalues of $\bar{\bar{\boldsymbol{M}}}$.

Since the transformed velocity signal $\boldsymbol{u}(t)$ is no longer a control input, a desired velocity signal, denoted by $\boldsymbol{u}_d(t)$, is designed based on (98) as follows:

$$\boldsymbol{u}_d = \boldsymbol{u}_a - k_2\boldsymbol{z}. \tag{113}$$

Because the dynamic model (110) can be expressed in terms of $\boldsymbol{u}_d(t)$ and then linearly parametrized, we see that

$$\bar{\bar{\boldsymbol{M}}}\dot{\boldsymbol{u}}_d + \bar{\bar{\boldsymbol{C}}}\boldsymbol{u}_d + \bar{\bar{\boldsymbol{R}}} = \boldsymbol{Y}_d(\boldsymbol{u}_d, \dot{\boldsymbol{u}}_d, \tilde{\boldsymbol{q}}, \theta, \boldsymbol{\eta}_r)\,\boldsymbol{\vartheta}, \quad (114)$$

where

$$\boldsymbol{\vartheta} = \begin{bmatrix} m & I & \mu_s m & \mu_l m \end{bmatrix}^T \quad (115)$$

is a vector of dynamical parameters and

$$\boldsymbol{Y}_d(\boldsymbol{u}_d, \dot{\boldsymbol{u}}_d, \tilde{\boldsymbol{q}}, \theta, \boldsymbol{\eta}_r) = \begin{bmatrix} y_{d11} & y_{d21} & y_{d31} & y_{d41} \\ y_{d12} & y_{d22} & y_{d32} & y_{d42} \end{bmatrix} \quad (116)$$

denotes a known regression matrix which is a function of the desired transformed velocity and acceleration. To simplify the control law, it is assumed that the friction coefficients are the same for each wheel, i.e., $\mu_{li} = \mu_l$ and $\mu_{si} = \mu_s$.

It is clear that since the dynamical parameters of the SSMR are not precisely determined, the actual vector $\boldsymbol{\vartheta}$ is uncertain. Defining the difference between this parameter vector and the parameter vector $\boldsymbol{\vartheta}_0$ that denotes the best-guess estimate for the unknown parameters in (115), we deduce that

$$\tilde{\boldsymbol{\vartheta}} = \boldsymbol{\vartheta}_0 - \boldsymbol{\vartheta}, \quad (117)$$

where

$$\boldsymbol{\vartheta}_0 = \begin{bmatrix} m_0 & I_0 & \mu_{s0} m_0 & \mu_{t0} m_0 \end{bmatrix}^T. \quad (118)$$

Assuming that $\tilde{\boldsymbol{\vartheta}}$ is bounded it is possible to find a coefficient ρ which fulfils the following inequality:

$$\left\|\tilde{\boldsymbol{\vartheta}}\right\| \leq \rho. \quad (119)$$

To develop a control law on the dynamic level, a new velocity signal error is defined (Dixon *et al.*, 2001; Mazur, 2001; Kozłowski and Majchrzak, 2002; Kozłowski and Pazderski, 2003):

$$\tilde{\boldsymbol{u}} = \boldsymbol{u}_d - \boldsymbol{u}. \quad (120)$$

The differential equations governing the transformed errors w and $\tilde{\boldsymbol{z}}$ for the closed-loop system have the following form:

$$\dot{w} = -k_1 w + \boldsymbol{u}_a^T \boldsymbol{J}\tilde{\boldsymbol{z}} + \tilde{\boldsymbol{u}}^T \boldsymbol{J}\boldsymbol{z}, \quad (121)$$

$$\dot{\tilde{\boldsymbol{z}}} = -k_2\tilde{\boldsymbol{z}} + w\boldsymbol{J}\boldsymbol{u}_a + \tilde{\boldsymbol{u}}. \quad (122)$$

A detailed derivation of the closed-loop error system can be found in (Dixon *et al.*, 2001).

For stability analysis, the following Lyapunov function candidate is proposed:

$$V_2(w, \tilde{\boldsymbol{z}}, \tilde{\boldsymbol{u}}) = \frac{1}{2}w^2 + \frac{1}{2}\tilde{\boldsymbol{z}}^T\tilde{\boldsymbol{z}} + \frac{1}{2}\tilde{\boldsymbol{u}}^T\bar{\bar{\boldsymbol{M}}}\tilde{\boldsymbol{u}}. \quad (123)$$

Taking the time derivative of V_2 yields

$$\dot{V}_2(w, \tilde{\boldsymbol{z}}, \tilde{\boldsymbol{u}}) = w\dot{w} + \tilde{\boldsymbol{z}}^T\dot{\tilde{\boldsymbol{z}}} + \tilde{\boldsymbol{u}}^T\bar{\bar{\boldsymbol{M}}}\dot{\tilde{\boldsymbol{u}}} + \frac{1}{2}\tilde{\boldsymbol{u}}^T\dot{\bar{\bar{\boldsymbol{M}}}}\tilde{\boldsymbol{u}}. \quad (124)$$

Calculating the term $\bar{\bar{\boldsymbol{M}}}\dot{\tilde{\boldsymbol{u}}}$ from (110) and using (121), (122) and then (108) in (124), we conclude that

$$\begin{aligned}\dot{V}_2(w, \tilde{\boldsymbol{z}}, \tilde{\boldsymbol{u}}) &= \dot{V}_1(w, \tilde{\boldsymbol{z}}) + \tilde{\boldsymbol{u}}^T\Big(w\boldsymbol{J}\boldsymbol{z} + \tilde{\boldsymbol{z}} + \bar{\bar{\boldsymbol{M}}}\dot{\boldsymbol{u}}_d \\ &\quad + \bar{\bar{\boldsymbol{C}}}\boldsymbol{u} + \bar{\bar{\boldsymbol{R}}} - \bar{\bar{\boldsymbol{B}}}\boldsymbol{\tau} + \frac{1}{2}\dot{\bar{\bar{\boldsymbol{M}}}}\tilde{\boldsymbol{u}}\Big). \end{aligned} \quad (125)$$

It is easy to prove that $\dot{\bar{\bar{\boldsymbol{M}}}} = \bar{\bar{\boldsymbol{C}}} + \bar{\bar{\boldsymbol{C}}}^T$. Using this relationship and adding and subtracting the term $\frac{1}{2}\tilde{\boldsymbol{u}}^T\bar{\bar{\boldsymbol{C}}}\tilde{\boldsymbol{u}}$ to the right-hand side of (125), the following equation is obtained:

$$\begin{aligned}\dot{V}_2(w, \tilde{\boldsymbol{z}}, \tilde{\boldsymbol{u}}) &= -k_1 w^2 - k_2\tilde{\boldsymbol{z}}^T\tilde{\boldsymbol{z}} \\ &\quad + \tilde{\boldsymbol{u}}^T\left(w\boldsymbol{J}\boldsymbol{z} + \tilde{\boldsymbol{z}} + \bar{\bar{\boldsymbol{M}}}\dot{\boldsymbol{u}}_d + \bar{\bar{\boldsymbol{C}}}\boldsymbol{u}_d + \bar{\bar{\boldsymbol{R}}} - \bar{\bar{\boldsymbol{B}}}\boldsymbol{\tau}\right) \\ &\quad + \frac{1}{2}\tilde{\boldsymbol{u}}^T\left(\bar{\bar{\boldsymbol{C}}}^T - \bar{\bar{\boldsymbol{C}}}\right)\tilde{\boldsymbol{u}}. \end{aligned} \quad (126)$$

Since $\bar{\bar{\boldsymbol{C}}}^T - \bar{\bar{\boldsymbol{C}}}$ is a skew-symmetric matrix, we see that

$$\tilde{\boldsymbol{u}}^T\left(\bar{\bar{\boldsymbol{C}}}^T - \bar{\bar{\boldsymbol{C}}}\right)\tilde{\boldsymbol{u}} = 0. \quad (127)$$

Using (127), the time derivative of the Lyapunov function can be rewritten as

$$\begin{aligned}\dot{V}_2(w, \tilde{\boldsymbol{z}}, \tilde{\boldsymbol{u}}) &= -k_1 w^2 - k_2\tilde{\boldsymbol{z}}^T\tilde{\boldsymbol{z}} \\ &\quad + \tilde{\boldsymbol{u}}^T\Big(w\boldsymbol{J}\boldsymbol{z} + \tilde{\boldsymbol{z}} + \bar{\bar{\boldsymbol{M}}}\dot{\boldsymbol{u}}_d + \bar{\bar{\boldsymbol{C}}}\boldsymbol{u}_d + \bar{\bar{\boldsymbol{R}}} - \bar{\bar{\boldsymbol{B}}}\boldsymbol{\tau}\Big). \end{aligned} \quad (128)$$

Now, making use of (114) in (128) results in

$$\begin{aligned}\dot{V}_2(w, \tilde{\boldsymbol{z}}, \tilde{\boldsymbol{u}}) &= -k_1 w^2 - k_2\tilde{\boldsymbol{z}}^T\tilde{\boldsymbol{z}} \\ &\quad + \tilde{\boldsymbol{u}}^T\left(w\boldsymbol{J}\boldsymbol{z} + \tilde{\boldsymbol{z}} + \boldsymbol{Y}_d\boldsymbol{\vartheta} - \bar{\bar{\boldsymbol{B}}}\boldsymbol{\tau}\right). \end{aligned} \quad (129)$$

To achieve robustness to the parametric uncertainty $\tilde{\boldsymbol{\vartheta}}$, an additional control input $\boldsymbol{\tau}_a$ is introduced. Based on (128), the following control law is proposed:

$$\boldsymbol{\tau} = \bar{\bar{\boldsymbol{B}}}^{-1}\left(w\boldsymbol{J}\boldsymbol{z} + \tilde{\boldsymbol{z}} + \boldsymbol{Y}_d\boldsymbol{\vartheta}_0 + \boldsymbol{\tau}_a + k_3\tilde{\boldsymbol{u}}\right). \quad (130)$$

According to (Spong, 1992; Dixon *et al.*, 2001), the term $\boldsymbol{\tau}_a$ is defined as

$$\boldsymbol{\tau}_a = \boldsymbol{Y}_d\frac{\rho^2\boldsymbol{Y}_d^T\tilde{\boldsymbol{u}}}{\left\|\boldsymbol{Y}_d^T\tilde{\boldsymbol{u}}\right\|\rho + \epsilon_2}, \quad (131)$$

where ϵ_2 is a positive constant scalar which can be set up as arbitrarily small.

Remark 3. It is clear that the function $\boldsymbol{\tau}_a$ in (131) is always time differentiable if so is $\|\boldsymbol{Y}_d^T\tilde{\boldsymbol{u}}\|$. This property is different from the typical robust control term used in (Spong, 1992) and allows us to limit the chattering of the control signal. It is an important property because it offers a possibility to use a classical backstepping approach.

Using (130) and (117) in (129), we have

$$\begin{aligned}\dot{V}_2\left(w,\tilde{\boldsymbol{z}},\tilde{\boldsymbol{u}}\right) &= -k_1w^2-k_2\tilde{\boldsymbol{z}}^T\tilde{\boldsymbol{z}}-\tilde{\boldsymbol{u}}^Tk_3\tilde{\boldsymbol{u}} \\ &\quad+\left(\boldsymbol{Y}_d^T\tilde{\boldsymbol{u}}\right)^T\left(\tilde{\boldsymbol{\vartheta}}-\frac{\rho^2\boldsymbol{Y}_d^T\tilde{\boldsymbol{u}}}{\left\|\boldsymbol{Y}_d^T\tilde{\boldsymbol{u}}\right\|\rho+\epsilon_2}\right).\end{aligned} \tag{132}$$

After some simple calculations, we can prove the following inequality:

$$\begin{aligned}\dot{V}_2\left(w,\tilde{\boldsymbol{z}},\tilde{\boldsymbol{u}}\right) &\le -k_1w^2-k_2\tilde{\boldsymbol{z}}^T\tilde{\boldsymbol{z}}-k_3\tilde{\boldsymbol{u}}^T\tilde{\boldsymbol{u}} \\ &\quad+\frac{\left\|\boldsymbol{Y}_d^T\tilde{\boldsymbol{u}}\right\|\rho\epsilon_2}{\left\|\boldsymbol{Y}_d^T\tilde{\boldsymbol{u}}\right\|\rho+\epsilon_2}.\end{aligned} \tag{133}$$

Since the last term in (133) is bounded,

$$0\le\frac{\left\|\boldsymbol{Y}_d^T\tilde{\boldsymbol{u}}\right\|\rho\epsilon_2}{\left\|\boldsymbol{Y}_d^T\tilde{\boldsymbol{u}}\right\|\rho+\epsilon_2}\le\epsilon_2, \tag{134}$$

we finally get

$$\dot{V}_2\left(w,\tilde{\boldsymbol{z}},\tilde{\boldsymbol{u}}\right)\le-k_1w^2-k_2\tilde{\boldsymbol{z}}^T\tilde{\boldsymbol{z}}-\tilde{\boldsymbol{u}}^Tk_3\tilde{\boldsymbol{u}}+\epsilon_2. \tag{135}$$

3.6. Control Law on the Motor Level

In this section the control law considering the drive model which was presented in Section 2.3 is developed.

Calculating $\boldsymbol{i}_a$ from (58) and then taking its time derivative, we get

$$\frac{\mathrm{d}}{\mathrm{d}t}\boldsymbol{i}_a=\left(2k_in\right)^{-1}\dot{\boldsymbol{\tau}}. \tag{136}$$

Next, using (136) in (59), we obtain

$$\boldsymbol{u}_{va}=L_a\left(k_in\right)^{-1}\dot{\boldsymbol{\tau}}+2R_a\boldsymbol{i}_a+2k_en\boldsymbol{\omega}_w. \tag{137}$$

Rearranging the terms in (137), we have

$$\dot{\boldsymbol{\tau}}=L_a^{-1}k_in\left(\boldsymbol{u}_{va}-2R_a\boldsymbol{i}_a-2k_en\boldsymbol{\omega}_w\right). \tag{138}$$

Here it is assumed that the voltage is the control signal of the drive system. Therefore, based on (130), the following desired torque signal $\boldsymbol{\tau}_d$ is designed:

$$\boldsymbol{\tau}_d=\bar{\bar{\boldsymbol{B}}}^{-1}\left(w\boldsymbol{J}\boldsymbol{z}+\tilde{\boldsymbol{z}}+\boldsymbol{Y}_d\boldsymbol{\vartheta}_0+\boldsymbol{\tau}_a+k_3\tilde{\boldsymbol{u}}\right), \tag{139}$$

where $\boldsymbol{\tau}_a$ is defined by (131).

The next step of the backstepping procedure consists in defining an error torque signal (see Kozłowski and Majchrzak, 2002; Kozłowski and Pazderski, 2003) as follows:

$$\tilde{\boldsymbol{\tau}}=\boldsymbol{\tau}_d-\boldsymbol{\tau}, \tag{140}$$

where $\boldsymbol{\tau}$ denotes the actual torque signal. To determine the voltage control law on the motor level, the following Lyapunov function candidate is proposed:

$$\begin{aligned}V_3\left(w,\tilde{\boldsymbol{z}},\tilde{\boldsymbol{u}},\tilde{\boldsymbol{\tau}}\right)&=\frac{1}{2}w^2+\frac{1}{2}\tilde{\boldsymbol{z}}^T\tilde{\boldsymbol{z}}+\frac{1}{2}\tilde{\boldsymbol{u}}^T\bar{\bar{\boldsymbol{M}}}\tilde{\boldsymbol{u}}+\frac{1}{2}\tilde{\boldsymbol{\tau}}^T\tilde{\boldsymbol{\tau}}\\&=V_2+\frac{1}{2}\tilde{\boldsymbol{\tau}}^T\tilde{\boldsymbol{\tau}}.\end{aligned} \tag{141}$$

Calculating its time derivative and using (125), (140) and (141), we get

$$\begin{aligned}\dot{V}_3\left(w,\tilde{\boldsymbol{z}},\tilde{\boldsymbol{u}}\right)&=\dot{V}_1\left(w,\tilde{\boldsymbol{z}}\right)\\&\quad+\tilde{\boldsymbol{u}}^T\left(w\boldsymbol{J}\boldsymbol{z}+\tilde{\boldsymbol{z}}+\bar{M}\dot{\mathbf{u}}_\mathbf{d}+\bar{\bar{\mathbf{C}}}\mathbf{u}_\mathbf{d}+\bar{\bar{\mathbf{R}}}-\bar{\bar{\mathbf{B}}}\boldsymbol{\tau}_\mathbf{d}\right)\\&\quad+\tilde{\boldsymbol{u}}^T\bar{\bar{\boldsymbol{B}}}\tilde{\boldsymbol{\tau}}+\tilde{\boldsymbol{\tau}}^T\dot{\tilde{\boldsymbol{\tau}}}.\end{aligned} \tag{142}$$

In order to design the control voltage $\boldsymbol{u}_{va}$, it is imposed that the following inequality is satisfied:

$$\tilde{\boldsymbol{u}}^T\bar{\bar{\boldsymbol{B}}}\tilde{\boldsymbol{\tau}}+\tilde{\boldsymbol{\tau}}^T\dot{\tilde{\boldsymbol{\tau}}}\le0. \tag{143}$$

Next, using (138) in (143), we get

$$\begin{aligned}&\tilde{\boldsymbol{u}}^T\bar{\bar{\boldsymbol{B}}}\tilde{\boldsymbol{\tau}}\\&\quad+\tilde{\boldsymbol{\tau}}^T\left[\dot{\boldsymbol{\tau}}_d-L_a^{-1}k_in\left(\boldsymbol{u}_{va}-2R_a\boldsymbol{i}_a-2k_en\boldsymbol{\omega}_w\right)\right]\le0.\end{aligned} \tag{144}$$

Based on (144), the following control law on the voltage level is proposed:

$$\boldsymbol{u}_{va}=L_a\left(k_in\right)^{-1}\left(\dot{\boldsymbol{\tau}}_d+k_4\tilde{\boldsymbol{\tau}}+\bar{\bar{\boldsymbol{B}}}^T\tilde{\boldsymbol{u}}\right)+R_a\boldsymbol{i}_a+k_en\boldsymbol{\omega}_w, \tag{145}$$

where k_4 is an adjustable positive coefficient.

Using (145) in (141), we obtain

$$\dot{V}_3\left(w,\tilde{\boldsymbol{z}},\tilde{\boldsymbol{u}},\tilde{\boldsymbol{\tau}}\right)=\dot{V}_2\left(w,\tilde{\boldsymbol{z}},\tilde{\boldsymbol{u}}\right)-k_4\tilde{\boldsymbol{\tau}}^T\tilde{\boldsymbol{\tau}}. \tag{146}$$

After the substitution of (135) in (146), the following inequality can be obtained:

$$\dot{V}_3\left(w,\tilde{\boldsymbol{z}},\tilde{\boldsymbol{u}}\right)\le-k_1w^2-k_2\tilde{\boldsymbol{z}}^T\tilde{\boldsymbol{z}}-k_3\tilde{\boldsymbol{u}}^T\tilde{\boldsymbol{u}}-k_4\tilde{\boldsymbol{\tau}}^T\tilde{\boldsymbol{\tau}}+\epsilon_2. \tag{147}$$

Now choose the parameter k_3 high enough such that

$$\forall t > 0 \; k_3 \geq \max\{k_1, k_2, k_4\} \frac{1}{m_2}, \qquad (148)$$

where m_2 is an upper bound of the function $m_2(w, \boldsymbol{z})$ which appears in (112). We have

$$k_{\min}\left(\frac{k_1}{k_{\min}}w^2 + \frac{k_2}{k_{\min}}\tilde{\boldsymbol{z}}^T\tilde{\boldsymbol{z}} + \frac{k_3}{k_{\min}}\tilde{\boldsymbol{u}}^T\tilde{\boldsymbol{u}} + \frac{k_4}{k_{\min}}\tilde{\boldsymbol{\tau}}^T\tilde{\boldsymbol{\tau}}\right) \geq k_{\min}\left(w^2 + \tilde{\boldsymbol{z}}^T\tilde{\boldsymbol{z}} + \tilde{\boldsymbol{u}}^T\bar{\bar{\boldsymbol{M}}}\tilde{\boldsymbol{u}} + \tilde{\boldsymbol{\tau}}^T\tilde{\boldsymbol{\tau}}\right), \qquad (149)$$

where $k_{\min} = \min\{k_1, k_2, k_4\}$. Next, combining (141) and (147) gives

$$\dot{V}_3(w, \tilde{\boldsymbol{z}}, \tilde{\boldsymbol{u}}, \tilde{\boldsymbol{\tau}}) \leq -\gamma V_3(w, \tilde{\boldsymbol{z}}, \tilde{\boldsymbol{u}}, \tilde{\boldsymbol{\tau}}) + \epsilon_2, \qquad (150)$$

where $\gamma = 2\min\{k_1, k_2, k_4\}$. Since all signals in the controller and the vehicle model are bounded (it is proved by Dixon *et al.*, 2001; Kozłowski and Majchrzak, 2002), we have $\dot{V}_3 \in \mathscr{L}_\infty$. Consequently,

$$V_3(w, \tilde{\boldsymbol{z}}, \tilde{\boldsymbol{u}}, \tilde{\boldsymbol{\tau}}) \leq V_3(0, \boldsymbol{0}, \boldsymbol{0}, \boldsymbol{0})\exp(-\gamma t) + \frac{\epsilon_2}{\gamma}\left[1 - \exp(-\gamma t)\right]. \qquad (151)$$

Using the fact that the transformation matrix $\boldsymbol{P}$ is always invertible, the following result was proved:

Theorem 2. *Assuming that the desired trajectory is selected to be bounded (cf. (65)) for all times $t \geq 0$ and the conditions (60), (119) are fulfilled, the proposed control law given by (98)–(102), (139) and (145) ensures the position and orientation tracking error to be globally uniformly ultimately bounded as follows:*

$$\|\tilde{\boldsymbol{q}}\| \leq \sqrt{\beta_1 \exp(-\gamma_1 t) + \epsilon_2\beta_2} + \beta_3 \exp(-\gamma_2 t) + \beta_4\epsilon_1, \qquad (152)$$

where γ_1, γ_2, β_1, β_2, β_3 and β_4 are positive constants.

4. Simulation Results

To validate the performance of the developed control law, simulation results using the *Matlab/Simulink* environment are presented. The model of the SSMR is based on a real construction of a small experimental mobile robot consisting of two MiniTracker-3 robots designed by Jedwabny *et al.* (2004). The friction surface is characterized by the functions $\mu_s(X, Y)$ and $\mu_t(X, Y)$ describing the friction coefficients. The values of the friction coefficients are related to the actual position of the COM of the robot (see Fig. 10). All parameters of the model and the default parameters of the controller are collected in Table 1.

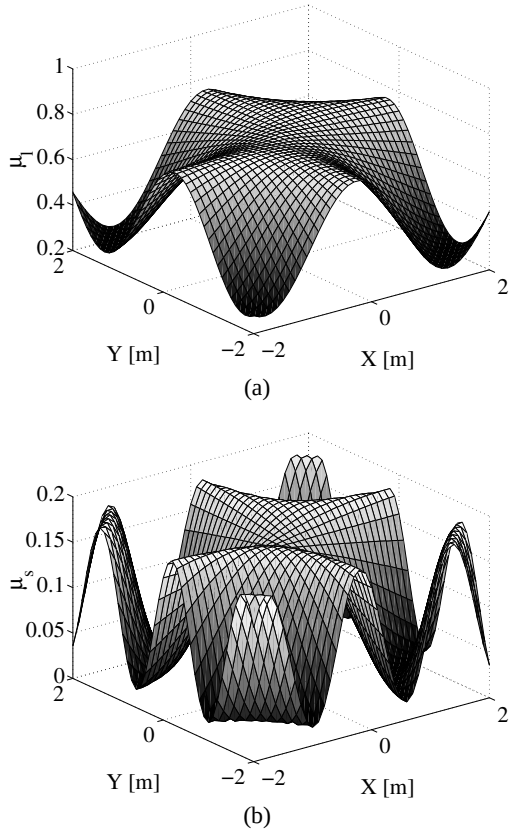

Fig. 10. Friction coefficients: (a) $\mu_l(X, Y)$, (b) $\mu_s(X, Y)$.

Table 1. Model and controller parameters.

Kinematic	$a = b = 39\,[\text{mm}]$, $c = 34\,[\text{mm}]$, $r = 26.5\,[\text{mm}]$
Dynamic	$m = 1\,[\text{kg}]$, $I = 0.0036\,[\text{kg}\cdot\text{m}^2]$
Motors	$L_a = 0.22\,[\text{mH}]$, $R_a = 3.9\,[\Omega]$, $k_e = 8.52\,\left[\frac{\text{mV}\cdot\text{s}}{\text{rad}}\right]$, $k_i = 8.55\,\left[\frac{\text{mN}\cdot\text{m}}{\text{A}}\right]$, $n = 12$, $\lvert i_{a\max}\rvert = 1.2\,[\text{A}]$, $\lvert u_{va\max}\rvert = 12\,[\text{V}]$
Surface	$\mu_l \in \langle 0.2, 0.8\rangle$, $\mu_s \in \langle 0.02, 0.18\rangle$
Default controller parameters	$k_1 = 1$, $k_2 = 1$, $k_3 = 5$, $k_4 = 2$, $\alpha_1 = 0.5$, $\epsilon_1 = 0.01$, $\epsilon_2 = 0.02$, $x_0 = -15\,[\text{mm}]$, $\rho = 2$, $\mu_{l0} = 0.5$, $\mu_{s0} = 0.1$, $m_0 = 1.2\,[\text{kg}]$, $I_0 = 0.0054\,[\text{kg}\cdot\text{m}^2]$

First, the regulation problem is examined for a kinematic and a dynamic controller (without a motor model). The torque signal is limited and cannot achieve a value greater than $0.25\,[\text{Nm}]$. The worst case is assumed when the robot should reach the posture $\boldsymbol{q}_r = [\ 0 \quad 0 \quad 0\ ]^T$ parallel to its initial position $\boldsymbol{q}(0) = [\ 0 \quad 1 \quad 0\ ]^T$, i.e., $z_1 = 0$, $z_2 = 0$ and $w \neq 0$.

In Fig. 11(a) the obtained paths are illustrated with respect to the initial value of the oscillator signal $\boldsymbol{z}_d$. It shows that the phase shift between z_{d1} and z_{d2} plays a very important role and influences the transient stages.

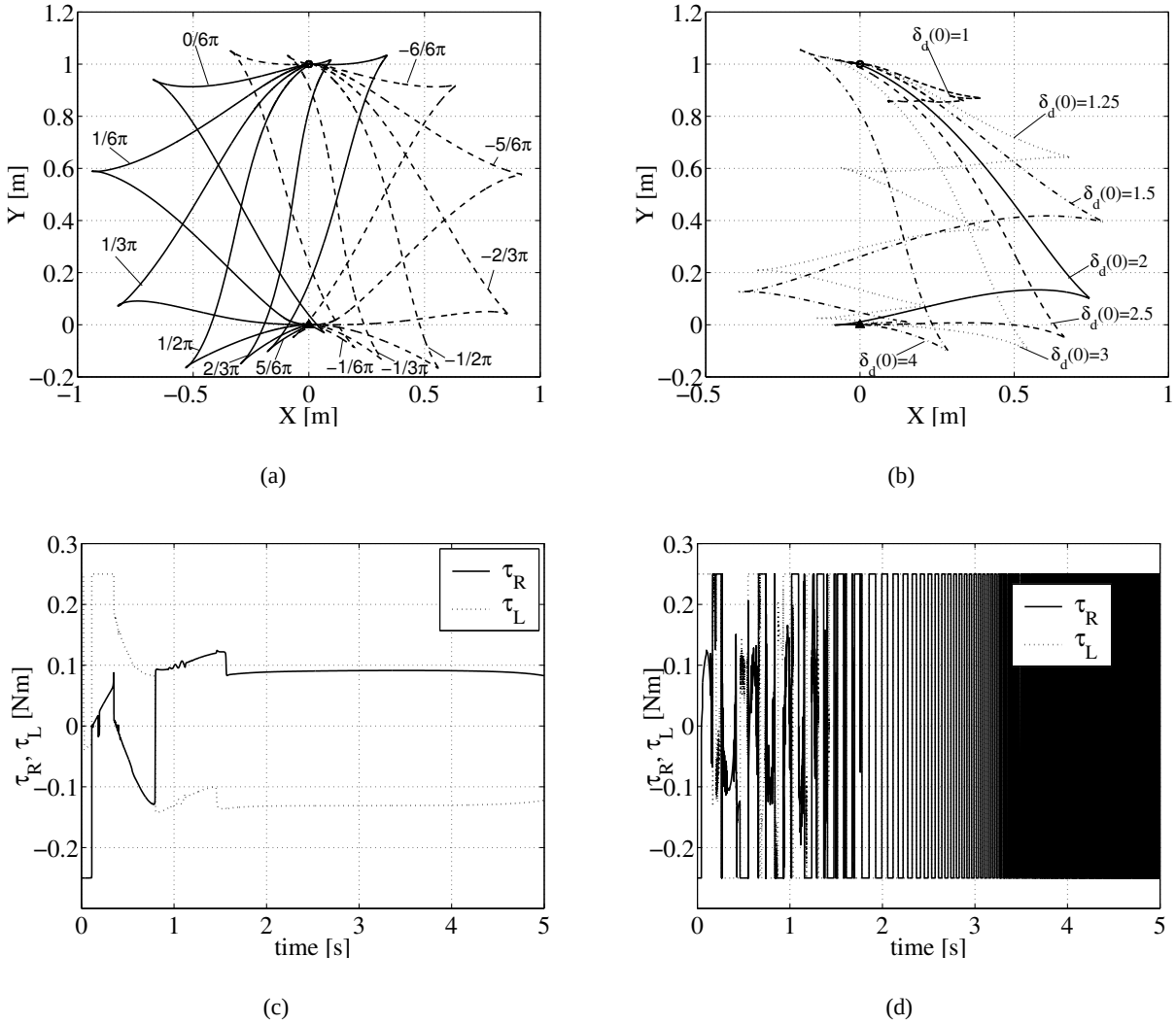

Fig. 11. Examination of the controller with respect to $\boldsymbol{z}_d\,(0)$: (a) Performed path with respect to φ, (b) Performed path with respect to $\delta_d\,(0)$, (c) Torque signal for $\delta_d\,(0) = 2.5$, and (d) Torque signal for $\delta_d\,(0) = 1$.

Therefore, the initial value $\boldsymbol{z}_d\,(0)$ can be tuned to obtain the best regulation performance from an energetic point of view, which results in the minimization of the number of changes in the direction movement. From Fig. 11(b) it can be seen that the initial value of $\delta_d\,(0)$ should not be too low, since it demands high values of control signals (cf. (98)–(100)). The limitation of the control signal results in signal chattering with a high frequency and, as a consequence, the regulation goal may not be reached (for example, see the path for $\delta_d\,(0) = 1$ presented in Fig. 11(b) and the torque signal for $\delta_d\,(0) = 1$ and $\delta_d\,(0) = 2.5$ in Figs. 11(c) and 11(d)). It is not sensible to force the controller to reduce the regulation error too fast by assuming a high value of α_1.

Second, a full dynamic model with motors is examined. The following parameters of the controller have been changed with respect to the default settings: $k_1 = 0.5$, $\alpha_1 = 0.3$, $\delta_d\,(0) = 2$, $\varphi = -7\pi/12$. In Fig. 12(a) the path and a series of postures of the robot at every 1 [s] of the simulation process are presented. From Fig. 12(b) it can be seen that the initial regulation error is highly reduced. The steady-state position and orientation errors are bounded as follows:

$$\text{for } t > 25\,[\text{s}]: \quad \left|\tilde{X}\right| < 1\,[\text{mm}], \quad \left|\tilde{Y}\right| < 0.5\,[\text{mm}] \quad \text{and} \quad \left|\tilde{\theta}\right| < 0.01\,[\text{rad}].$$

In Fig. 12(c) a comparison of signals $\boldsymbol{z}_d\,(0)$ and $\boldsymbol{z}\,(0)$ is presented in the three dimensional space. It can be observed that $\boldsymbol{z}\,(t)$ approaches the trajectory generated by the oscillator, i.e., $\boldsymbol{z}_d\,(t)$ indirectly determines the actual position and the orientation error. The voltage control signal for simulation is illustrated in Fig. 12(d): small chattering appears only during the initial stage of simulation when an auxiliary error $\tilde{\boldsymbol{z}}\,(t)$ is relatively high (see Fig. 12(c)).

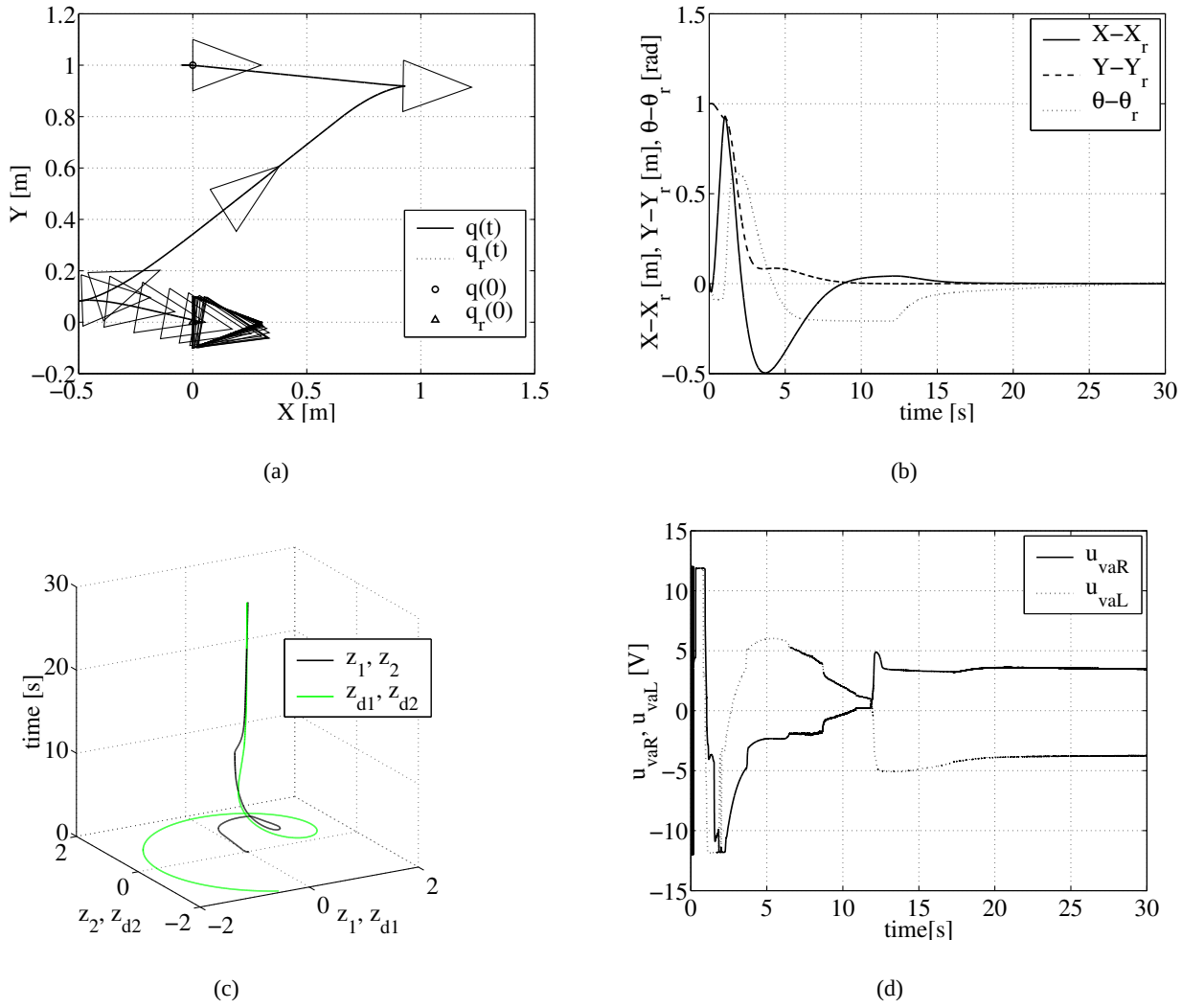

Fig. 12. Regulation case for $\tilde{\boldsymbol{q}}(0) = \begin{bmatrix} 0 & 1 & 0 \end{bmatrix}^T$: (a) Performed path, (b) Regulation errors, (c) Auxiliary error and oscillator signal, and (d) Voltage signal.

The results of the next simulation are obtained for $\boldsymbol{q}_r = \begin{bmatrix} 0 & 0 & 0 \end{bmatrix}^T$, $\boldsymbol{q}(0) = \begin{bmatrix} 0 & 1 & -\pi \end{bmatrix}^T$, $k_1 = 1$, $\alpha_1 = 0.5$, $\delta_d(0) = 3.2$, $\varphi = \pi$. In Figs. 13(a)–(d), the path, regulation errors, auxiliary signals and voltage signals are shown. The regulation errors are bounded as follows:

$$\text{for } t > 25\,[\text{s}]: \quad \left|\tilde{X}\right| < 10\,[\text{mm}], \quad \left|\tilde{Y}\right| < 1\,[\text{mm}] \quad \text{and} \quad \left|\tilde{\theta}\right| < 0.05\,[\text{rad}].$$

It is easy to observe that if $\tilde{\boldsymbol{z}}(0)$ is relatively small, this controller allows us to obtain good transient states and to rapidly limit motion changes. Therefore, choosing $\boldsymbol{z}_d(0)$ should be considered for a practical implementation of the control law.

Next, numerical simulations concern the trajectory tracking problem. For the results presented in Figs. 14(a)–(e) the following parameters were assumed: $k_1 = 2$, $\alpha_1 = 0.3$, $\delta_d(0) = 1.7$, $\varphi = \pi/12$. The reference trajectory is as follows:

$$X_r(t) = \left(\frac{1}{1+0.2t}\cos 0.2t - 1\right)\,[\text{m}],$$

$$Y_r(t) = \frac{1}{1+0.2t}\sin 0.2t\,[\text{m}],$$

while $\theta_r(t)$ is calculated by the reference model (64). The steady-state tracking errors are bounded as follows:

$$\text{for } t > 30\,[\text{s}]: \quad \left|\tilde{X}\right| < 5\,[\text{mm}], \quad \left|\tilde{Y}\right| < 4\,[\text{mm}] \quad \text{and} \quad \left|\tilde{\theta}\right| < 0.04\,[\text{rad}].$$

In Fig. 14(e) the friction coefficients are illustrated, but according to Figs. 14(b) and 14(c) it is clear that the error and velocity signals are almost invariant to disturbances.

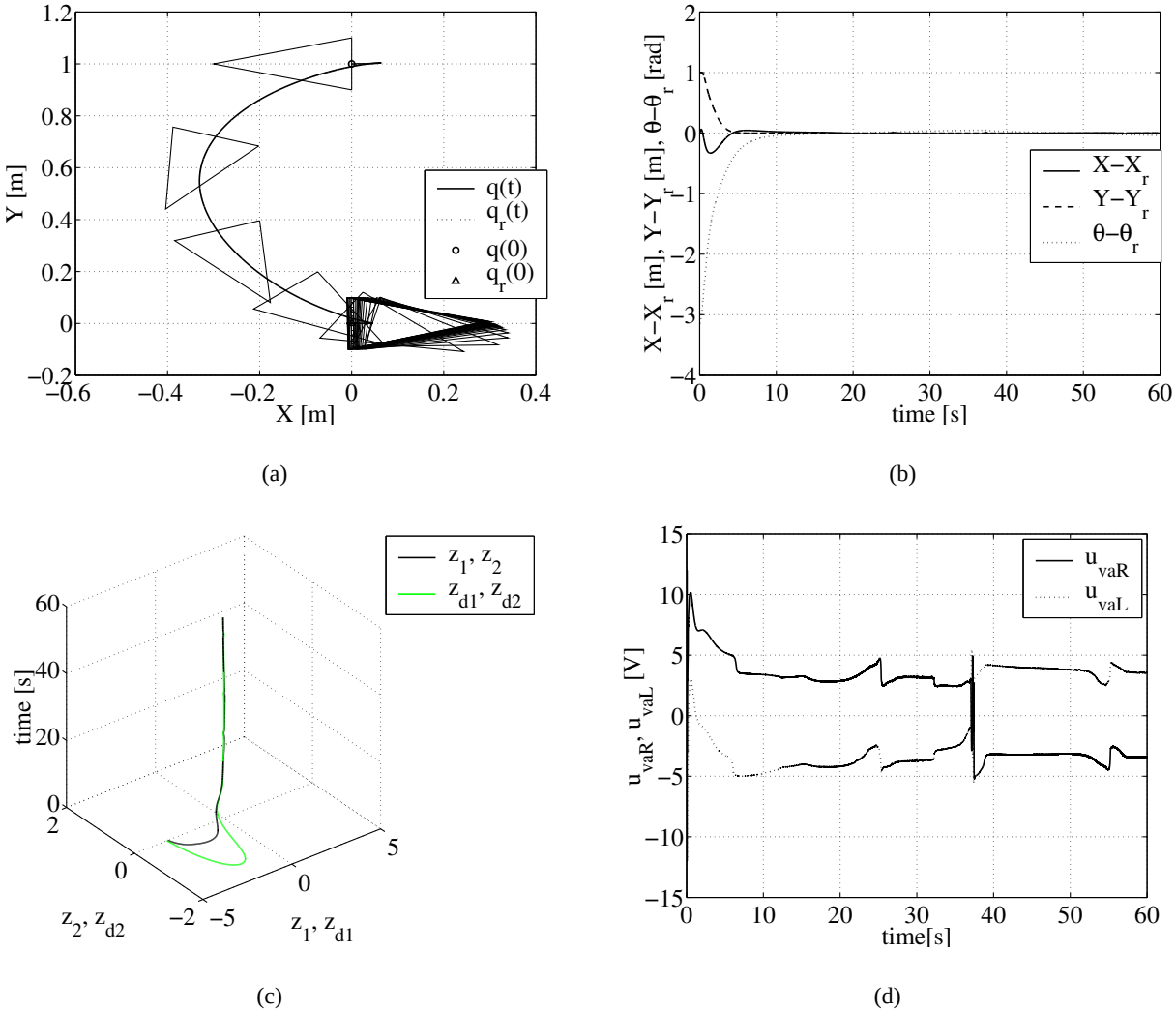

Fig. 13. Regulation case for $\tilde{\boldsymbol{q}}(0) = \begin{bmatrix} 0 & 1 & -\pi \end{bmatrix}^T$: (a) Performed path, (b) Regulation errors, (c) Auxiliary error and oscillator signal, and (d) Voltage signal.

In the next simulation experiment for the trajectory tracking problem the following reference trajectory was assumed:

$$X_r(t) = [(1 + 0.2\sin 0.9t)\cos 0.15t - 1]\ [\mathrm{m}], \quad (153)$$

$$Y_r(t) = (1 + 0.2\sin 0.9t)\sin 0.15t\,[\mathrm{m}]. \quad (154)$$

The parameters of the controller different from their default values are $k_3 = 10$, $k_4 = 10$, $\alpha_1 = 0.3$, $\delta_d(0) = 1.5$, $\varphi = -2\pi/3$. In this simulation experiment the following steady-state errors are recorded (cf. Fig. 15(b)):

$$\text{for } t > 20\,[\mathrm{s}]: \quad \left|\tilde{X}\right| < 12\,[\mathrm{mm}], \quad \left|\tilde{Y}\right| < 11\,[\mathrm{mm}] \quad \text{and} \quad \left|\tilde{\theta}\right| < 0.02\,[\mathrm{rad}].$$

It can be seen that the tracking errors are higher compared with previous simulations, since the dynamic properties concerning the inertia of the vehicle play an important role. In this case friction coefficients change in a significant range, too. Therefore it is necessary to increase the coefficient k_3 to improve the performance of the controller. It is interesting to see that although a trajectory tracking error exists, the reference and actual paths are almost the same (cf. Fig. 15(e)) in the final stage of simulation. The controlled robot is delayed with respect to the reference vehicle.

5. Conclusion

In this paper a new algorithm considering the kinematic, dynamic and drive model of a 4WD skid-steering mobile robot has been presented. To solve the kinematic problem we used the idea of a kinematic oscillator that gives

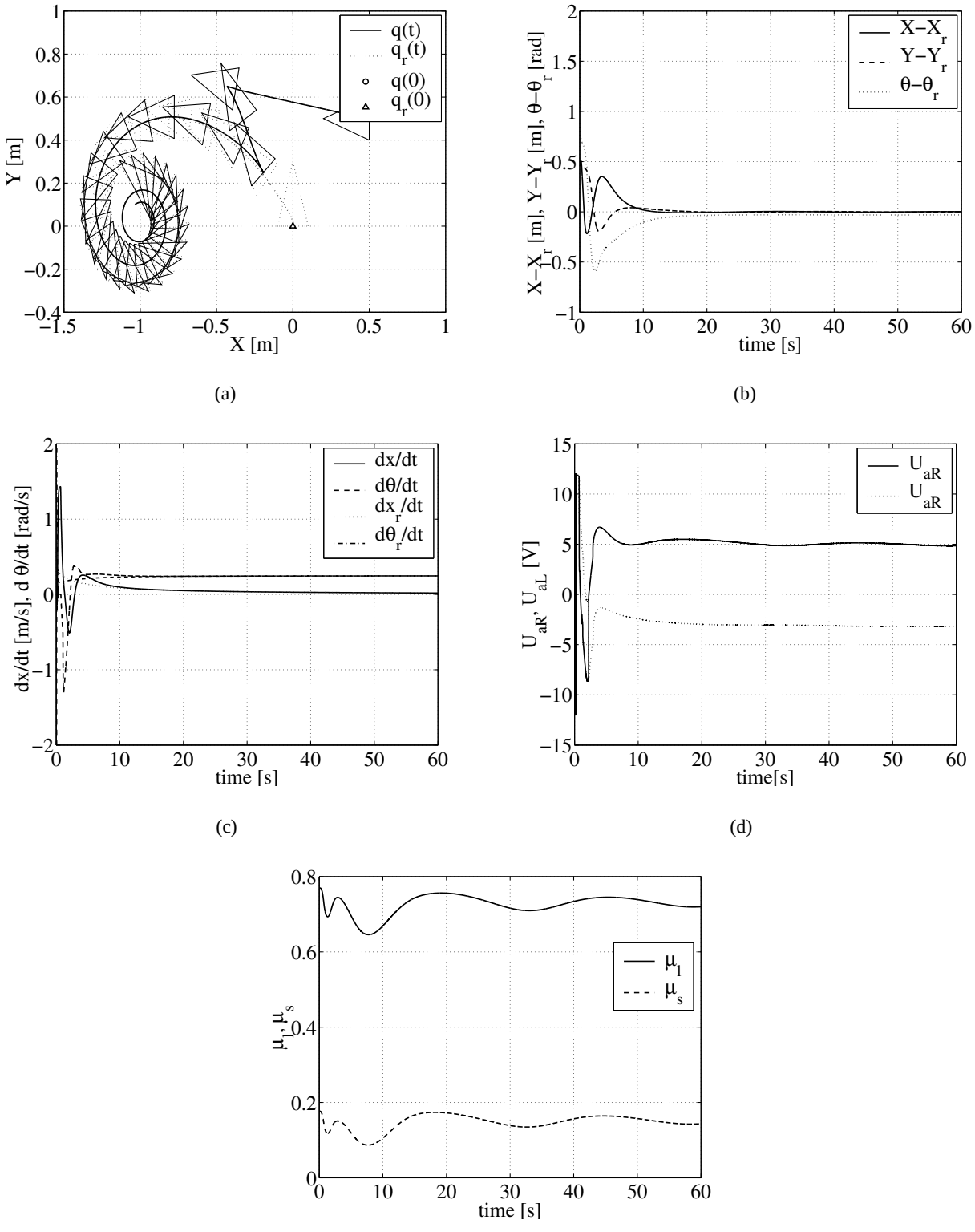

Fig. 14. Trajectory tracking case for $\tilde{\boldsymbol{q}}(0) = \begin{bmatrix} 0.5 & 0.5 & -\pi/2 \end{bmatrix}^T$: (a) Performed path, (b) Tracking errors, (c) Linear and angular velocities, (d) Voltage signal, and (e) Friction coefficients.

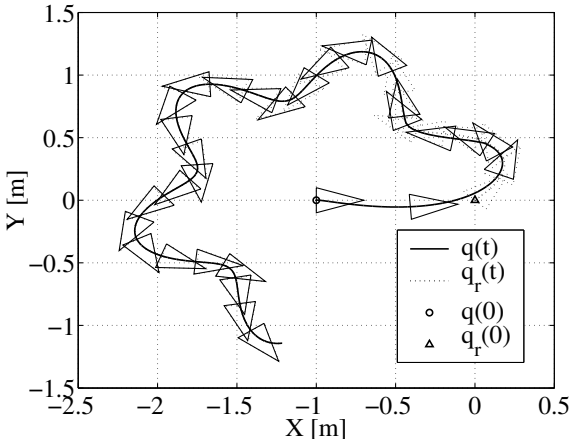

(a)

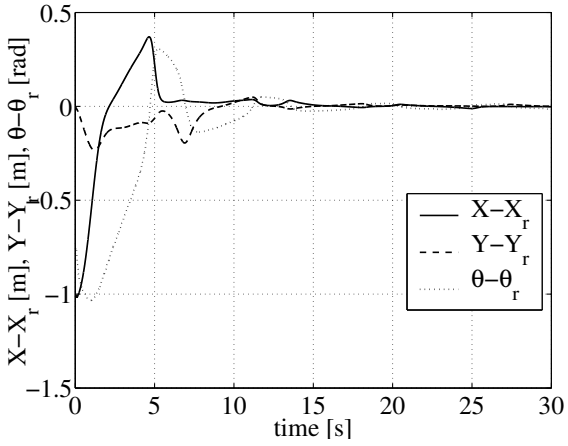

(b)

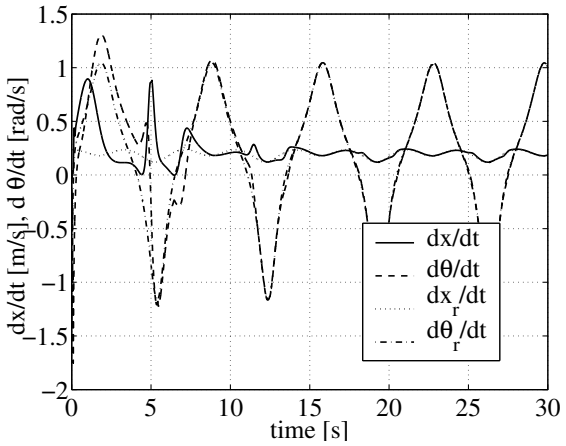

(c)

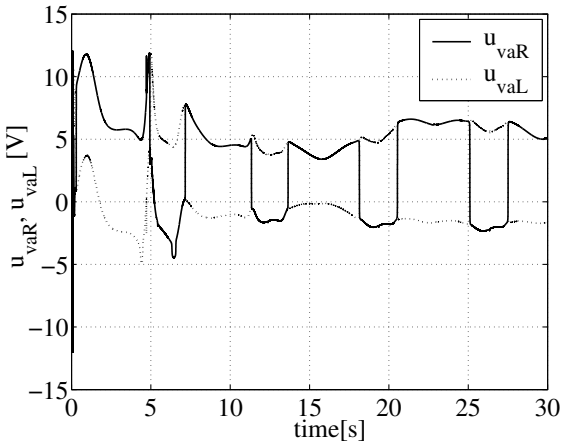

(d)

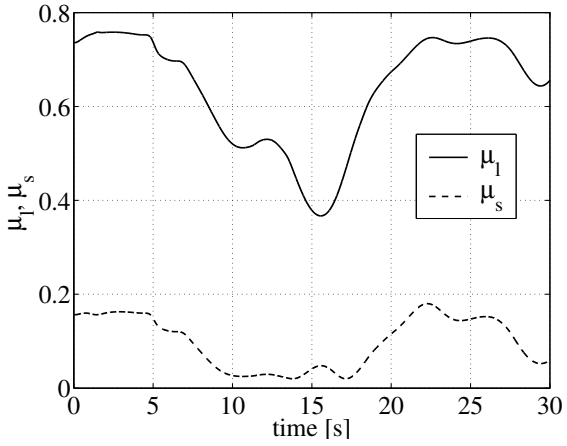

(e)

Fig. 15. Trajectory tracking case $\tilde{\boldsymbol{q}}(0) = \begin{bmatrix} -1 & 0 & -\pi/4 \end{bmatrix}^T$: (a) Performed path, (b) Tracking errors, (c) Linear and angular velocities, (d) Voltage signal, and (e) Friction coefficients.

a possibility to obtain practical stabilization in trajectory tracking and regulation problems. It was proved that the overall controller stabilizes the system asymptotically to certain bounds of the position and orientation tracking errors. The obtained convergence is exponential. In contrast to the previous work done by Caracciolo *et al.* (1999), the presented approach is characterized by better robustness to dynamic parameters uncertainty. Theoretical deliberations are illustrated by discussion how to tune the parameters of the controller.

Future work is devoted to the extension of this approach to other classes of nonholonomic systems which have the size of the state vector greater than three (e.g., a typical car drive kinematic model).

References

Brockett R.W. (1983): *Asymptotic stability and feedback stabilization*, In: Differential Geometric Control Theory (R.W. Brockett, R.S. Milman and H.J. Susmann, Eds.). — Boston: Birkhäuser, pp. 181–191.

Caracciolo L., De Luca A. and Iannitti S. (1999): *Trajectory tracking control of a four-wheel differentially driven mobile robot*. — IEEE Int. Conf. *Robotics and Automation*, Detroit, MI, pp. 2632–2638.

Campion G., Bastin G. and D'Andrea-Novel B. (1996): *Structural properties and classification of kinematic and dynamic models of wheeled mobile robots*. — IEEE Trans. Robot. Automat., Vol. 12, No. 1, pp. 47–62.

Dixon W.E., Dawson D.M., Zergeroglu E. and Behal A. (2001): *Nonlinear Control of Wheeled Mobile Robots*. — London: Springer.

Dixon W.E., Behal A., Dawson D.M. and Nagarkatti S.P. (2003): *Nonlinear Control of Engineering Systems, A Lyapunov-Based Approach*. — Boston: Birkhäuser.

Gutowski R. (1971): *Analytic Mechanics*. — Warsaw: Polish Scientific Publishers, (in Polish).

De Luca A. and Oriolo G. (1995): *Modeling and control of nonholonomic mechanical systems*, In: Kinematics and Dynamics of Multi-Body Systems (J. Angeles and A. Kecskeméthy, Eds.). — CISM Lecture Notes, No. 360, Wien: Springer, pp. 277–342.

Mazur A. (2001): *Control algorithms for the kinematics and the dynamics of mobile manipulators: A comparative study*. — Arch. Contr. Sci., Vol. 11, No. 3–4, pp. 223–244.

Morin P. and Samson C. (2003): *Practical stabilization of driftless systems on Lie groups: The transverse function approach*. — IEEE Trans. Automat. Contr., Vol. 48, No. 9, pp. 1496–1508.

Morin P. and Samson C. (2002): *Feedback control of nonholonomic wheeled vehicles: A survey*. — Arch. Contr. Sci., Vol. 12, No. 48, pp. 7–36.

Murray R.M. and Sastry S. (1993): *Nonholonomic motion planning: Steering using sinusoids*. — IEEE Trans. Automat. Contr., Vol. 38, No. 5, pp. 700–716.

Jedwabny T., Kiełczewski M., Kowalski M., Ławniczak M., Michalski M., Michałek M., Pazderski D. and Kozłowski K. (2004): *Nonholonomic mobile robot MiniTracker research and educational purposes*. — Proc. 35-th Int. Symp. *Robotics*, Paris, France, pp. 254–259.

Kozłowski K. and Majchrzak J. (2002): *A new control algorithm for a nonholonomic mobile robot*. — Arch. Contr. Sci., Vol. 12, No. 48, pp. 37–69.

Kozłowski K. and Pazderski D. (2003): *Control of a four-wheel vehicle using kinematic oscillator*. — Proc. 6-th Int. Conf. *Climbing and Walking Robots and their Supporting Technologies, CLAWAR 2003*, Catania, Italy, pp. 135–146.

Pacejka H.B. (2002): *Tyre and Vehicle Dynamics*. — Oxford: Butterworth-Heinemann.

Pazderski D., Kozłowski K. and Dixon W.E. (2004): *Tracking and regulation control of a skid steering vehicle*. — Amer. Nuclear Soci, 10-th Int. Topical Meeting *Robotics and Remote Systems*, Gainesville, Florida, USA, pp. 369–376.

Spong M.W. (1992): *On the robust control of robot manipulators*. — IEEE Trans. Automat. Contr., Vol. 37, No. 11, pp. 1782–1786.